International Journal of Plasticity 148 (2022) 103141

Contents lists available at ScienceDirect

International Journal of Plasticity

journal homepage: www.elsevier.com/locate/ijplas

Evolving dislocation cores at Twin Boundaries: Theory of CRSS Elevation

Orcun Koray Celebi [a,#], Ahmed Sameer Khan Mohammed [a,#], Jessica A. Krogstad [b], Huseyin Sehitoglu [a,*]

[a] Department of Mechanical Science and Engineering, University of Illinois at Urbana-Champaign, 105 S. Mathews Ave., Urbana, IL 61801, USA
[b] Department of Materials Science and Engineering, University of Illinois at Urbana-Champaign, 1304 W. Green St., Urbana, IL 61801, USA

ARTICLE INFO

Keywords:
Twin Boundaries
Dislocation core
Dislocation reaction
Slip transfer
Nanotwinned materials

ABSTRACT

Superior mechanical response of twinnable materials fundamentally arises from an elevation of Critical Resolved Shear Stresses (CRSS) due to Dislocation-Twin Boundary (D-TB) reactions. These reactions exhibit rich variety with several possible outcomes and exhibit complex dependence on microstructural properties, causing state-of-the-art models to adopt a case-by-case simulation of each reaction relying on empirical potentials or twin-interaction parameters. We develop an analytical "Evolving Dislocation Core" (EDC) model devoid of empiricism, capable of predicting the CRSS-elevation for any reaction, given the microstructural properties (elastic constants, twin crystallography, etc.). The approach is fundamentally rooted in energy-minimization within a fully-anisotropic framework revealing the evolution of dislocation cores with progression of the reaction. The core-structure of complex dislocations (e.g. stair-rod) in the reaction is proposed, for the first time in literature, as a non-planar composite of disregistries distributed on slip and twin planes. The model is applied to multiple slip-incorporation reactions in several Face-Centered-Cubic (FCC) materials (Pb, Ag, Cu, Ni-Co alloys and Ni-Ti alloys and high-entropy alloy FeNiCoCrMn). The predicted CRSS-elevations show agreement with atomistic simulations (Ni) and experiment (FeNiCoCrMn). The model further establishes a strong correlation of the elevation with unstable stacking/twinning fault energy and the magnitude of the sessile dislocation's Burgers vector, while revealing poor correlation with the stable intrinsic stacking fault energy which is a common benchmark. Thus the analytical EDC model developed in this study advances understanding of slip-twin interactions on multiple fronts while serving as an effective predictive model for CRSS-elevation instrumental in materials design.

1. Introduction

Mechanical behavior of materials is a macroscopic manifestation of fundamental mechanisms at the microstructural level. These mechanisms predominantly involve activity of crystalline defects such as point defects (e.g. vacancies, solutes), line defects (slip dislocations), and surface defects (e.g. free surfaces, twin boundaries, and grain boundaries) in the material. Onset of their activity and their mutual interaction during progression of material deformation have critical implications on mechanical performance metrics

* Corresponding author. Tel: +1 217 333 4112
E-mail address: huseyin@illinois.edu (H. Sehitoglu).
# Both authors contributed equally to this paper.

https://doi.org/10.1016/j.ijplas.2021.103141
Received 2 September 2021; Received in revised form 17 October 2021;
Available online 1 November 2021

such as flow stress, strength, fracture toughness, and fatigue resistance. One of the major classes of such microstructural phenomena is the interaction of slip dislocations with Twin Boundaries (TB). These interactions are complex phenomena encompassing several possible routes and outcomes exemplifying the wide variety of behavioral responses that materials can exhibit on a microstructural level. Dislocation – Twin Boundary (D-TB) interactions can either result in blockage of the incoming slip at the TB or result in a "dislocation reaction" where the incoming slip can transform into distinct product dislocations (Ezaz et al., 2011; Hartley and Blachon, 1978; Mahajan and Chin, 1973; Müllner and Solenthaler, 1997; Robertson et al., 2005; Samaee et al., 2021; Sangid et al., 2011). Such interactions effectively emulate a barrier to dislocation motion to elevate local CRSS (Critical Resolved Shear Stress) of active slip systems in the material (Rémy, 1981). This elevation manifests as desirable enhancements in strength (Chowdhury et al., 2016; Rémy, 1981; Sim et al., 2017; Valentino et al., 2021), strain-hardening (Bönisch et al., 2018; Steinmetz et al., 2013), dynamic Hall-Petch behavior (Bouaziz and Guelton, 2001; Zhao et al., 2020), and particularly a marked improvement in fatigue resistance (Alkan et al., 2016; Alkan and Sehitoglu, 2017; Bönisch et al., 2018; Brenne et al., 2020; Chowdhury et al., 2013; Rémy, 1981; Sidharth et al., 2020a). Dislocation reactions also play a critical role in functional materials such as Shape Memory Alloys (SMAs), dictating the rate of slip emission from disconnections on internal twin boundaries (Brenne et al., 2020; Mohammed and Sehitoglu, 2020, 2021), ultimately manifesting in the damping and fatigue response of SMAs (Sidharth et al., 2020a; Sidharth et al., 2021; Sidharth et al., 2020b).

Understanding D-TB reactions has been a subject of interest over the past five decades (Bönisch et al., 2018; Chassagne et al., 2011; Chou, 1966; Kaschner et al., 2007; Lee et al., 1989; Mahajan, 1971; Mahajan and Chin, 1973; Rémy, 1977, 1981; Solenthaler, 1990; Steinmetz et al., 2013; Xu et al., 2016; Yamakov et al., 2003). The earliest studies were dedicated to evidencing individual dislocation reactions through microscopy (optical and electron microscopy) and crystallographic analysis, establishing the Burgers vectors of dislocations involved in the reactions (Kaschner et al., 2007; Lee et al., 1990; Li et al., 2011; Mahajan and Chin, 1973; Rémy, 1977, 1981; Solenthaler, 1990). Subsequently, models were developed to quantify how the D-TB reaction elevates the CRSS of the incoming slip system (Gu et al., 2014a; Jin et al., 2008; Jin et al., 2006; Shabib and Miller, 2009; Zhu et al., 2007; Zhu et al., 2011). The first analytical models recognized that the incoming slip system approaching the TB encounters additional resistance in the form of an elastic "image interaction force" (Alkan and Sehitoglu, 2017; Chen et al., 2007; Hirth and Lothe, 1983) thereby elevating the CRSS. This force however encounters a singularity at the intersection of the dislocation at the TB pushing the elevation to infinity which is unphysical and not observed. Removal of the singularity required consideration of the dislocation as an entity of finite "core-width" where non-continuum atomistic forces operate across its slip plane (alternatively thought of as the plane of "disregistry") (Pacheco and Mura, 1969). Similar models were also successfully developed to model interactions of "cross-slip" in Face-Centered Cubic (FCC) materials, capturing effects such as core-recombination of separated Shockley partials and core-redistribution on cross-slipped planes (Bonneville and Escaig, 1979; Püschl, 2002; Püschl and Schoeck, 1993; Ramírez et al., 2012; Schoeck, 2001, 2009). And yet, the efficacy of these approaches is limited to a specific type of D-TB interaction, with a special character of the incoming dislocation (screw character) transmitting through the TB, and further limited by assumptions of isotropic constitutive relation for the material. On the contrary, D-TB reactions exist in several classes with rich variety, requiring an improved framework to model them while necessitating a more realistic representation of the underlying material's elastic constitution.

The advent of computational simulation techniques such as Molecular Dynamics (MD) (Chassagne et al., 2011; Chowdhury et al., 2014; Ezaz et al., 2011; Sangid et al., 2012; Wang et al., 2012; Wang et al., 2017; Yamakov et al., 2003) and Dislocation-Dynamics (DD) (Fan et al., 2021; Imrich et al., 2014; Wei et al., 2019; Zhang et al., 2021) bolstered the development of a distinct class of approaches capable of handling a variety of D-TB reactions. Several studies focused on the simulation of reactions within such computational frameworks, more commonly from atomic-scale MD, seeking to quantify the magnitude of CRSS-elevation achievable. These approaches are currently the state-of-the-art to model D-TB reactions and are still challenged by two major caveats:

- These frameworks involve some form of empiricism, either for the interatomic force-fields (in the case of MD) or dislocation mobilities (in the case of DD). Consequently, predictions of these models are strongly limited by the physical fidelity of these empirical parameters, dictating whether a D-TB reaction can even be successfully simulated and if the dislocation-core atomistic forces or elastic anisotropy are reliably captured.
- These methods approach the problem as a case-by-case analysis of each individual type of reaction, requiring carefully constructed, often expensive simulations. Consequently, predictions on one simulated reaction cannot be reliably extended to other reactions without them being simulated explicitly. Also, such simulations cannot reliably reveal dependencies of the observed elevation on underlying microstructural and material properties such as load orientation, fault energies, and elastic anisotropy.

Furthermore, even from successful simulations, the predicted CRSS-elevations are often unphysically high, typically in the ranges of few GPa in MD simulations (Xu et al., 2016; Yamakov et al., 2003). In fact, one of the lowest predictions, to the best of the authors' knowledge, was a threshold for slip-transmission proposed to be ~400 MPa for all D-TB interactions (Chassagne et al., 2011; Gu et al., 2014a; Zhu et al., 2007). While convenient and effective, such a fixed threshold for all D-TB interactions irrespective of material properties can be prohibitively conservative in either prediction of material behavior or in materials design. In summary, current approaches to model D-TB reactions would significantly benefit from a unifying framework capable of modeling a large variety of reactions, with predictability unmarred by any empiricism and capable of capturing material properties such as anisotropy at the continuum scale and atomistic potential energies at dislocation cores. Atomistic potential energies such as the Generalized Stacking Fault Energy (GSFE) and Generalized Planar Fault Energy (GPFE) must be considered to capture changes in the dislocation core during the reaction. The current study develops such a predictive framework, named as the "Evolving Dislocation Core" (EDC) model, for D-TB reactions and shows its efficacy by application to multiple reactions and materials. The only material parameters involved are elastic constants and fault-energetics which can be reliably obtained from *ab initio* DFT methods (Gengor et al., 2021; Zimmerman

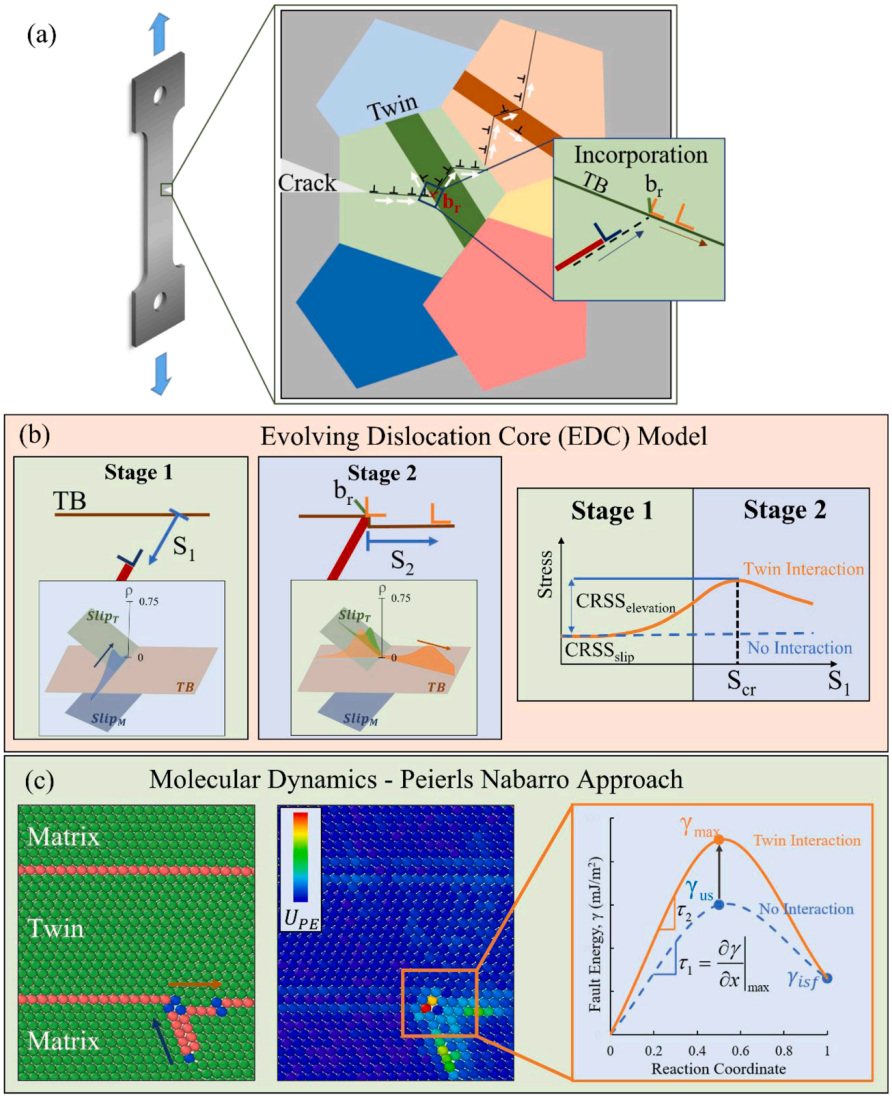

Fig. 1. (a) Critical role of slip-twin interactions in mechanical response of materials, particularly at the front of a short crack in fatigue and fracture; D-TB interactions at twins within equiaxed grains are schematically shown (b) Overview of the EDC model as applied to the slip-incorporation D-TB reaction, highlighting the two-stage methodology; the first stage captures the approach of the leading partial and the second stage captures the formation of the stair-rod dislocation and the incorporated twinning dislocation; the distributed cores of these dislocations are indicated and the variation of the CRSS across both stages are indicated with and without twin interaction (c) Overview of the Molecular Dynamics (MD) approach - A Control-Volume (CV) + Peierls-Nabarro (PN) approach is proposed, tracking the variation of fault energies at a small control volume surrounding the core of the dislocations participating in the slip-incorporation reaction; the Peierls-Nabarro model predicts the CRSS through a gradient of the varying energies at the dislocation cores

et al., 2000).

Further, there is a knowledge gap in the scientific understanding of D-TB reactions that the authors would like to address. One of the reasons for reaction complexity is the formation of several sessile dislocations with unconventional Burgers vectors. For instance, in the best-studied FCC system, dislocation interactions form several locks (e.g., $a/2\langle 110\rangle$ Lomer-Cottrell lock) and stair-rod dislocations (typically in slip-incorporation reactions, e.g. $a/3\langle 010\rangle$) (Ezaz et al., 2011; Hirth and Lothe, 1983; Lee et al., 2013). To the best of the author's knowledge, there is no understanding of the core structure of these dislocations. In the authors' opinion, this knowledge-gap on the core structure of sessile dislocations is the primary impediment to the development of a predictive analytical approach. The best example which shows the value and impact of such understanding is the evolution of the field of Non-Schmid behavior in Body-Centered Cubic (BCC) metals (Alkan et al., 2017; Vitek, 1992). The non-planar spreading of disregistry distributions constituted the fundamental scientific cause for a perplexing macro-scale slip behavior (Alkan et al., 2018a; Duesbery and Vitek, 1998). The proposed model hypothesizes a core-structure for such sessile dislocations motivated by the non-planar distributed cores observed in BCC materials. The success of this modeling hypothesis is demonstrated by the good agreement of model-predicted critical stresses with atomic-scale simulations and also experiments.

The EDC model is elaborated by application to the "slip incorporation" reaction which is one of the most common D-TB interactions

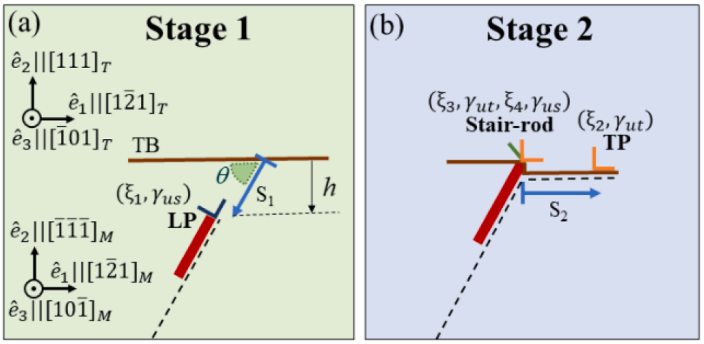

Fig. 2. Stages in the Evolving Dislocation Cores (EDC) model proposed in this study: (a) Crystallography of the twin (T) and matrix (M) is indicated; the $a/6\langle 112\rangle$ Leading Partial (LP) ahead of the stacking fault (bold red line) in the $a/2\langle 011\rangle$ extended dislocation approaches the TB;θ represents the angle between the slip plane and the TB, s_1 represents the position of the incoming partial and h is the normal distance of the partial away from the TB (b) Formation of stair-rod dislocation and the incorporated Twinning Partial (TP) gliding on the TB

in FCC materials. In these materials, lattice dislocations with Burgers vectors $a/2\langle 011\rangle$ (where a is the FCC lattice constant) dissociate into an extended dislocation consisting of two Shockley partials with Burgers vectors $a/6\langle 112\rangle$ separated by a stacking fault (Hirth and Lothe, 1983). As the extended dislocation approaches the twin, the leading Shockley partial reacts with the TB and forms an incorporated twinning dislocation that subsequently glides along the TB (alternatively viewed as getting "incorporated" on the TB) while also forming a sessile dislocation on the TB called the stair-rod dislocation (refer Fig. 1). There are several distinct reactions within this family and even within the same material. For instance, there are 12 linearly independent Burgers vectors possible for the incoming leading partial and for each leading partial there are 6 distinct incorporated twinning partials possible on the TB, yielding a total of 72 possible slip-incorporation reactions. The sessile stair-rod dislocations forming in these reactions also vary, forming with different Burgers vector magnitudes and core structures. For each reaction, the CRSS-elevation realized can significantly vary depending on the orientation of applied external load and twin crystallography (Ezaz et al., 2011). With such combinatorial complexity, it becomes prohibitively challenging to conduct simulations within frameworks such as MD/DD for each reaction under varying loading conditions to model the CRSS-elevation, necessitating a predictive ground-up approach as proposed in this study. Thus in these regards, the incorporation reaction poses all the challenges associated with reaction variety and complex microstructural dependence offered by D-TB interactions in general and is thus an apt study target for the EDC model. The methodology of the model is first elaborated for 3 slip-incorporation reactions and subsequently applied to 6 more reactions, illustrating its efficacy to capture all aforementioned complexities.

In the following sections, the methodology of the EDC model is elaborated. The predictions of the model are validated against atomistic simulations in Molecular Dynamics (MD). A modified approach involving a tracked Control-Volume (CV) around dislocation cores and the Peierls-Nabarro (PN) model is proposed, for the first time in literature, focusing on the atomic-scale energetics at the core of the simulated dislocations (refer Fig. 1). The methodology is presented with FCC Nickel (Ni) as the study target. This choice is informed by the reliability of the interatomic potentials developed for pure FCC materials over several years, ultimately serving as a reliable benchmark to validate the EDC model. Also, Ni is chosen to study Ni-based alloys such as Ni-Co and Ni-Ti, revealing the influence of enhanced twinnability in these alloys on the CRSS-elevations in slip-twin interactions. The model is also applied to several pure FCC materials and the high-entropy alloy FeNiCoCrMn establishing its wide applicability independent of the availability of empirical potentials for these materials. Multiple slip-incorporation reactions are modeled, and the variance of CRSS-elevation depending on the load orientation, stair-rod Burgers vector magnitude, and fault energy landscapes are established, significantly advancing state-of-the-art understanding in the field.

2. Modeling Methodology

The EDC model is elaborated in this section. Without loss of generalization, a pair of $\{111\}$ planes are chosen, one of them chosen to be the TB and the other the interacting slip system in the FCC crystal structure. The TB is chosen to be on a $(111)_M$ plane and the slip plane is chosen to be a $(1\bar{1}1)_M$ plane where the subscript M indicates that the indices are referenced to the matrix/parent phase. The crystallography is described in Fig. 2 (a). The global coordinate frame is given by the unit vector triad $\hat{e}_1 - \hat{e}_2 - \hat{e}_3$, with the vectors aligned with the following crystallographic directions in the matrix and twin: $\hat{e}_1 \parallel [1\bar{2}1]_M \parallel [1\bar{2}1]_T$, $\hat{e}_2 \parallel [\bar{1}\bar{1}\bar{1}]_M \parallel [111]_T$ and $\hat{e}_3 \parallel [10\bar{1}]_M \parallel [\bar{1}01]_T$ (Fig. 2). The target slip-incorporation reaction is first partitioned into two stages:

a Stage 1: Approach of the leading partial towards the TB. The leading partial will alternatively be referred to as the incident/incoming dislocation in this paper. During this stage, the leading partial faces resistance from the image interaction force associated with the D-TB interaction.
b Stage 2: Formation of the product dislocations i.e. the sessile stair-rod on the TB and the incorporated twinning dislocation gliding away from the stair-rod.

Table 1
Target slip-incorporation D-TB reactions modeled in this study under specified loading directions; the composition of the unconventional stair-rod Burgers vector ($\vec{b}_{SR}$) as a linear combination of conventional $a/6\langle 112\rangle$ slip ($\vec{b}_{SR-SP}$)/twin ($\vec{b}_{SR-TP}$) Burgers vector of the FCC system is given.

Loading Direction, $\hat{v}$ (Tension)	Reaction #	Reaction	Solution for stair-rod partitioning factors (λ)
$[010]_M$	I	$\frac{a}{6}[21\bar{1}]_M \rightarrow \frac{a}{6}[2\bar{1}\bar{1}]_M + \frac{a}{3}[010]_M$ Shockley partial $\vec{b}_{LP}$ — Twinning partial $\vec{b}_{TP}$ — Stair-rod $\vec{b}_{SR}$ $\lambda_3\frac{a}{6}[\bar{1}2\bar{1}]_M + \lambda_4\frac{a}{6}[\bar{1}\bar{2}\bar{1}]_T$ Twinning partial, $\vec{b}_{SR-TP}$ Shockley partial, $\vec{b}_{SR-SP}$	$\lambda_3 = 5/6$ $\lambda_4 = 1/2$
$[1\bar{2}3]_M$	II	$\frac{a}{6}[21\bar{1}]_M \rightarrow \frac{a}{6}[\bar{1}2\bar{1}]_M + \frac{a}{3}[3\bar{1}0]_M$ Shockley partial $\vec{b}_{LP}$ — Twinning partial $\vec{b}_{TP}$ — Stair-rod $\vec{b}_{SR}$ $\lambda_3\frac{a}{6}[1\bar{2}1]_M + \lambda_4\frac{a}{6}[\bar{2}\bar{1}1]_T$ Twinning partial, $\vec{b}_{SR-TP}$ Shockley partial, $\vec{b}_{SR-SP}$	$\lambda_3 = 2/3$ $\lambda_4 = 1$
$[11\bar{1}]_M$	III	$\frac{a}{6}[21\bar{1}]_M \rightarrow \frac{a}{6}[11\bar{2}]_M + \frac{a}{6}[101]_M$ Shockley partial $\vec{b}_{LP}$ — Twinning partial $\vec{b}_{TP}$ — Stair-rod $\vec{b}_{SR}$ $\lambda_3\frac{a}{6}[1\bar{2}1]_M + \lambda_4\frac{a}{6}[\bar{1}\bar{2}\bar{1}]_T$ Twinning partial, $\vec{b}_{SR-TP}$ Shockley partial, $\vec{b}_{SR-SP}$	$\lambda_3 = 1/6$ $\lambda_4 = 1/2$

In the current study, we analyze 3 distinct incorporation reactions under different loading orientations, as summarized in Table 1. The incident Leading Partial (LP) has a Burgers vector of $\vec{b}_{LP} = a/6[21\bar{1}]_M$ on its slip plane $(1\bar{1}1)_M$, with the matrix-twin crystallography chosen as shown in Fig. 2. The position of the incoming partial is given by s_1, taken along the direction of approach of the partial towards the TB. The core of the incoming partial is characterized by its "core-width" ξ_1, defined formally in Section 2.1.1. The core-width, ξ_1, is predominantly dictated by the unstable stacking fault energy (γ_{us}) on the GSFE curve corresponding to the incoming slip system. The position of the incorporated twinning partial, $\vec{b}_{TP}$, is given by s_2, taken along the TB moving away from the stair-rod. Its core is characterized by the core-width ξ_2, which depends on the unstable twinning fault energy barrier (γ_{ut}) on the GPFE curve corresponding to the active twinning system. The stair-rod dislocation has a non-conventional Burgers vector (of the type $a/3\langle 010\rangle$, $a/6\langle 310\rangle$ and $a/3\langle 101\rangle$) in that it does not correspond to either a slip or twin Burgers vector of the FCC matrix (which is of $a/6\langle 112\rangle$ type). Further, its core-structure has not been revealed or even hypothesized to date. In this study, we propose the stair-rod core

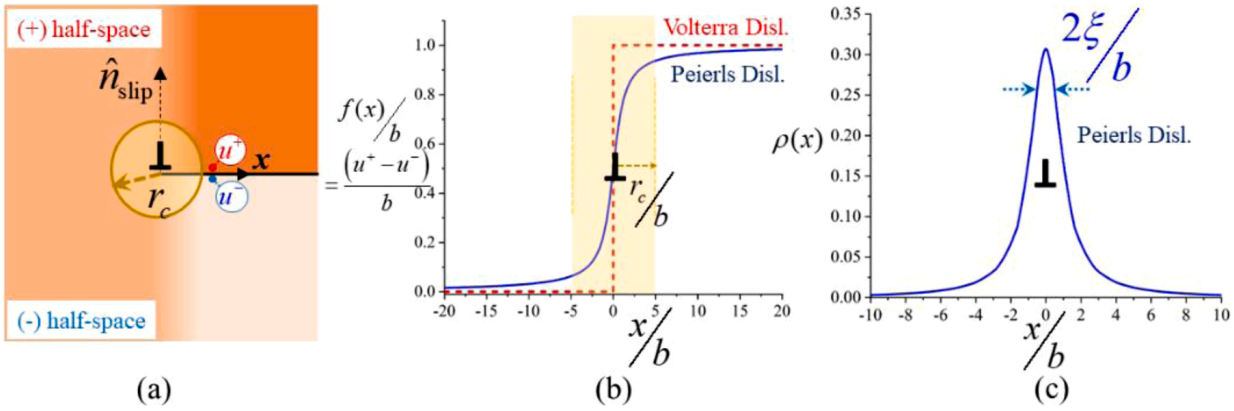

Fig. 3. Defining the dislocation core structure and core-width (a) Schematic of a dislocation in the continuum bulk; the slip plane, with normal $\hat{n}_{slip}$, partitions the space into two half-spaces; the disregistry between the two half-spaces is tracked along the slip plane by taking the difference of displacement components $u^{\pm}$ at the slip plane in the respective half-spaces; the region within $r_c = 5b$ is conventionally known as the "core" of the dislocation (b) Plot of the disregistry distribution for the Volterra dislocation model and the Peierls dislocation model; the "core" region demarcated by the cut-off $r_c = 5b$ is also indicated (c) Plot of the dislocation-density distribution of the Peierls dislocation, indicating the finite core-width, ξ (for the definition of core-width see the main text)

structure as a linear combination of fractional dislocations distributed on slip and twin planes of the parent crystal structure (FCC in this case). The unconventional Burgers vector is then interpreted as an additive composite of conventional $a/6\langle 112\rangle$ Burgers vectors in the FCC system (refer Table 1). The candidate $a/6\langle 112\rangle$ Burgers vectors that can form the stair-rod are among that of the incoming Shockley partial on the incident $(1\bar{1}1)_M$ slip plane, all twinning partials on the $(111)_M$ TB, and all Shockley partials on the $(1\bar{1}1)_T$ slip plane within the twin. Only these candidate Burgers vectors can have the same dislocation line (i.e. $\hat{e}_3 \| [10\bar{1}]_M$, refer Fig. 2 (b)) as that of the stair-rod formed in the incorporation reaction, and can hence compose the stair-rod's core structure. For each stair-rod, it can be verified that its linear decomposition into specific Burgers vectors from the aforementioned candidates is unique, for positive linear pre-factors $\lambda_{3,4} > 0$. For instance, in reaction I, the stair-rod $a/3[010]_M$ can only be constructed by a linear combination of the two Burgers vectors $a/6[\bar{1}2\bar{1}]_M$ and $a/6[\overline{121}]_T$. No other candidate Burgers vectors can combine to give this stair-rod Burgers vector. The linear pre-factors λ_3 and λ_4 attached to the constituting Burgers vectors can be solved for by equating each of the three crystallographic indices of the linear combination and the stair-rod dislocation. The linear decomposition of other stair-rod dislocations from reactions II and III are also listed in Table 1. The stair-rod core is consequently characterized by multiple core-widths (ξ_3 and ξ_4) and both the unstable stacking fault energy barrier (γ_{us}) and the unstable twinning fault energy barrier (γ_{ut}) as shown in Fig. 2. The positions and core-widths characterize all intermediate states in the reaction. The number of parameters is governed by the number of participating dislocations in the reaction, 4 in all considered cases of this study (refer Table 1). These parameters will be defined more formally with reference to the core structures of the dislocations in the following sections.

2.1. Evolving Dislocation Core Model Methodology

2.1.1. Core of a dislocation

We first specify what is meant by the "core" of a dislocation as referred to in this study. A brief description is presented here sufficient for the purposes of the study and the reader is referred to (Hirth and Lothe, 1983; Peierls, 1940) for comprehensive coverage on this concept. At the continuum or "macro"-scale, it is convenient to understand dislocations as line defects across which there is a displacement jump in the crystal structure. This displacement is along the Burgers vector, $\vec{b}$, of the dislocation with the jump occurring across the slip plane. To understand this jump further, we part the infinite crystal into two semi-infinite halves, a (+) half and a (-) half, split by the slip plane of the dislocation (Fig. 3). The normal to the slip plane $\hat{n}_{slip}$ is shown.

Define the displacement jump or disregistry as the difference in displacements between the two halves of the crystal taken at the slip plane, given by $(u^+ - u^-)$. The displacements, $u^{\pm}$, are resolved scalar components along the direction of the Burgers vector. Other components of the displacement can be ignored since they experience no jump across the dislocation. If this disregistry is tracked as we move across the dislocation (i.e. along x direction in Fig. 3 (a)) and plotted, then we get the disregistry profile plotted as a dashed-line in Fig. 3 (b). It is a step function that starts at zero prior to encountering the defect and subsequently jumps to the magnitude of the Burgers vector on the right. This model for a dislocation is also called the "Volterra" dislocation after one of the earliest definitions of dislocations in the continuum scale (Volterra, 1907).

The Volterra model reliably captures continuum displacement fields away from the center of the dislocation. At the center, the abrupt jump causes a singularity in the solutions for the displacement field, which is unphysical in nature. Because of the singularity, physical displacements around the center of the dislocation are not captured by the Volterra model. This region around the center is called the "core" of the dislocation and ascribed a radius of $r_c = 5\left|\vec{b}\right| = 5b$ from the center point (Hirth and Lothe, 1983). Thus, at distances larger than $r_c = 5b$ from the center, the Volterra model is a reliable model for the dislocation.

Although the Volterra model proves effective for elastic interactions at higher scales, consideration of the disregistry distribution at the core, equivalently referred to as the "core structure", is necessary to understand the core-evolution transforming reacting dislocations to product dislocations in dislocation reactions. The analytical solution for the disregistry distribution, $f(x)$, was derived by Peierls in (Peierls, 1940) (also elaborated in (Schoeck, 1994)) by solving an integro-differential force-equilibrium equation considering both elastic and atomistic forces at the core. This distribution is given by:

$$f(x) = b\left(\frac{1}{2} + \frac{1}{\pi}\tan^{-1}\left(\frac{x}{\xi}\right)\right) \tag{2.1}$$

where b is the magnitude of the Burgers vector of the dislocation, and ξ is known as the "core-width" of the dislocation. This model is referred to as the "Peierls dislocation" model and the disregistry function in Eq. (2.1) is plotted in Fig. 3 (b). The core disregistry can otherwise be thought of as "misfit" in the dislocation core. The core width can be better understood from the plot of the "dislocation density" distribution, which is a derivative of the disregistry function, given by:

$$\rho(x) = \frac{df(x)}{dx} = \frac{b}{\pi}\frac{\xi}{\left(x^2 + \xi^2\right)} \tag{2.2}$$

The dislocation-density distribution is plotted in Fig. 3 (c). The core-width, ξ, is indicated in the figure, representing the width of the dislocation density. This model of the dislocation is commonly referred to as the Peierls model of the dislocation, and will be used to model all dislocations in the D-TB interactions. It is worth noting that the direction of increasing x is aligned with the direction of increasing disregistry (i.e. direction of increasing f). Also, the center of the disregistry distribution and the dislocation density are at $x = 0$, which denotes the position of the dislocation. If x is chosen in the opposite sense to increasing disregistry and if the dislocation is at a position $x = s$ with respect to the origin, the equations for disregistry distribution and dislocation densities are modified as:

$$f(x) = b\left(\frac{1}{2} - \frac{1}{\pi}\tan^{-1}\left(\frac{x-s}{\xi}\right)\right); \rho(x) = -\frac{b\xi}{\pi\left((x-s)^2 + \xi^2\right)} \tag{2.3}$$

The above form of the disregistry and dislocation density will be used in Section 2.1.2 for Stage 2 of the EDC model. Note that away from the center of the core the dislocation density approaches zero i.e. $\rho(x) \to 0$ as $x \to \pm\infty$. It is worth realizing that for the Volterra model of the dislocation we have zero core-width and hence, in the limit of $\xi \to 0$, the disregistry function in (2.1) approaches the step-function in Fig. 3 (b).

2.1.2. Stage 1: Approach of incident dislocation and image interaction

In the first stage of the reaction, the incident leading partial moves towards the TB under the applied load, as schematically illustrated in Fig. 2. Thus its position, defined by s_1, starts at a large value (asymptotically at ∞) and reduces as it approaches the TB. In the regime $\infty > s_1 \gg r_c$, the D-TB interaction is elastic in nature, known as "image interaction" (Chou, 1966; Gemperlová, 1968; Pacheco and Mura, 1969). There is no atomistic interaction between the core of the dislocation and the TB. This regime is modeled by Stage 1 of the EDC model. The image interaction arises from the difference in elastic constitution between the parent phase where the dislocation resides and the elastically-distinct phase (twin) that the dislocation is approaching under applied load. Such a difference in elastic constitution can either arise from a difference in crystal orientation across the boundary (as in this case with a TB, also with grain boundaries), or due to difference in material elastic constants themselves (as in case of free surfaces or phase boundaries) (Bacon et al., 1980; Gemperlová, 1968). Consequently, the image interaction force on the dislocation is fundamentally dictated by the difference in continuum strain-energy of the dislocation when it is in the bulk matrix far away from the TB ($s_1 \to \infty$) as compared to when it is on the TB ($s_1 = 0$).

Thus, the calculation of image interaction force for Stage 1 of the EDC model only involves the continuum strain-energy of the dislocation. For this purpose, it is sufficient to model the dislocation as a Volterra dislocation (refer Section 2.1.1). The strain-energy of a Volterra dislocation (per unit length of the dislocation line) is given by the well-known analytical expression (Hirth and Lothe, 1983):

$$E^{\text{Volt.}}_{\text{strain}} = E\ln\frac{R}{r_c} \tag{2.4}$$

where E is a pre-logarithmic energy factor and R is the outer radial limit of integration in calculating the strain-energy. The image interaction can be calculated as a force per unit length of the dislocation line, $\overrightarrow{p}$, acting on the LP. It is given by:

$$\overrightarrow{p}(s_1) = \left(\frac{E^{\infty} - E^0}{h(s_1)}\right)\widehat{e}_2 \tag{2.5}$$

where $h(s_1) = s_1\sin\theta$ is the normal distance from the interface, for the known acute angle θ between the slip plane and twin plane (refer Fig. 2 (a)). E^{∞} and E^0 are pre-logarithmic energy factors when the dislocation is in the bulk matrix ($s_1 \to \infty$, far away from the TB) and when it is at the TB ($s_1 = 0$), respectively. For all cases considered in this study, we have $E^{\infty} \leq E^0$ implying that the TB repels the incoming LP. Calculations of E^{∞} and E^0 are elaborated in detail in Appendix A. The resolved stress on the slip plane, from the image interaction, repelling the LP away from the TB is given by:

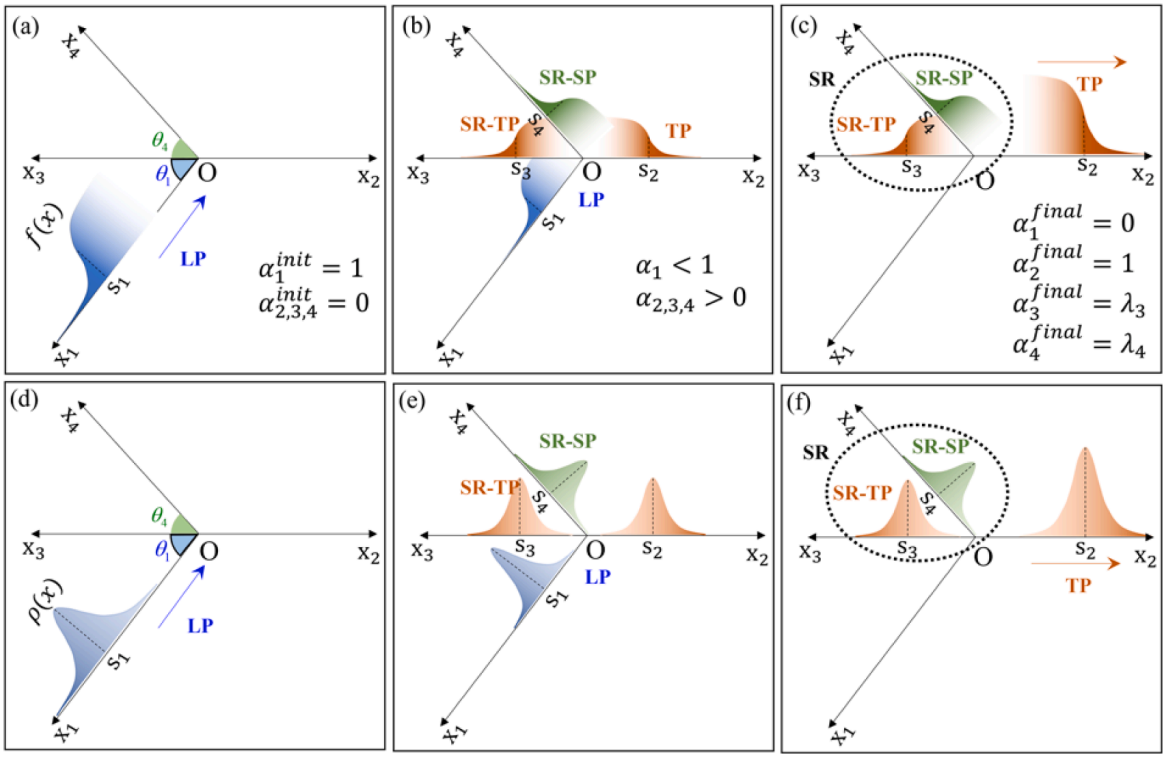

Fig. 4. Core-evolution in the D-TB reaction captured in Stage 2 of the EDC model (a) The disregistry function of the leading partial (LP) is plotted, approaching the TB as s_1 reduces, towards intersection point O; note the α_i ($i = 1,2,3,4$) pre-factors indicating that the core of the leading partial is complete/full ($\alpha_1^{\text{init.}} = 1$) and yet to evolve into other dislocation cores of the reaction ($\alpha_{2,3,4}^{\text{init.}} = 0$) (b) Core-evolution during the D-TB reaction leading to the formation of stair-rod (SR) and twinning partial (TP) dislocation cores ($\alpha_{2,3,4} > 0$) while the incident partial core recedes ($\alpha_1 < 1$) (c) Completion of the D-TB reaction indicated by the formation of the complete stair-rod (SR) dislocation core (composed of stair-rod Shockley partial (SR-SP), and the stair-rod twinning partial (SR-TP), and the incorporated twinning partial (TP); the pre-factors of all dislocations are now at their final values at completion, indicating the formation of the full twinning partial (TP) $\alpha_2^{\text{final}} = 1$, the stair-rod cores ($\alpha_{3,4}^{\text{final}} = \lambda_{3,4}$) at the expense of the incident partial's core ($\alpha_1^{\text{final}} = 0$); (d-f) show the corresponding evolution of the dislocation density distributions corresponding to (a-c) respectively

$$\tau_{\text{IMG}}(s_1) = \frac{p(s_1)}{b_{LP}} \sin\theta \qquad (\infty > s_1 \ll r_c) \tag{2.6}$$

where $p(s_1)$ is the magnitude of the image interaction force and b_{LP} is the Burgers vector magnitude of the incoming leading partial. Along with this resolved stress τ_{IMG}, the incoming partial also has to overcome the lattice friction stress, also known as the Peierls stress, arising from the atomistic energy barriers in the parent/matrix crystal structure. Consequently, the total CRSS required to move the dislocation towards the boundary is expressed as,

$$\tau_{\text{CRSS}}^{\text{I}}(s_1) = \tau_p^{LP} + \tau_{\text{IMG}}(s_1) \tag{2.7}$$

where τ_p^{LP} is the Peierls stress for the Shockley partial. The Peierls stress is calculated by considering the Peierls model of the dislocation core as described in Section 2.1.1, considering it to be in the bulk matrix sufficiently far away from the TB. A brief outline of the calculation is presented here and a detailed description is deferred to Appendix B. First, the equilibrium core-width of the Peierls dislocation is determined to be the one which minimizes the sum total of the continuum strain-energy of the dislocation and atomistic energy of planar disregistry within the dislocation core. Then the Peierls-Nabarro model is applied to calculate the misfit energy profile of the dislocation as it traverses the parent crystal structure by unit Burgers vector. The maximum gradient on this energy profile determines the Peierls stress corresponding to lattice friction.

Thus, in Stage 1, the CRSS $\tau_{\text{CRSS}}^{\text{I}}(s_1)$, given in Eq. (2.7), gradually elevates as the incoming partial approaches the TB. However, note that $\tau_{\text{CRSS}}^{\text{I}}(s_1)$ encounters a singularity as $s_1 \to 0$. This is unphysical in nature and is caused by the fact that the image-interaction formulation does not account for the finite dislocation core of the dislocation and the atomistic core-interactions with the TB when the incident partial is very close to it (i.e. when $s_1 \leq r_c$). These interactions are captured in stage 2 of the EDC model. In stage 2, as the incoming partial approaches close to the TB, the unknown core-widths ξ are determined for all participating dislocations in the reaction, capturing the evolution of the incoming partial's core into cores of the product dislocations in the reaction. This is elaborated further below.

2.1.3. Stage 2: Interaction with TB and core-evolution into product dislocations

The second stage of the EDC model captures the crucial part of the D-TB interaction where the dislocation core of the incident partial interacts with the TB eventually reacting to form product dislocations i.e. the stair-rod and the incorporated twinning partial in the slip-incorporation reaction. Thus, in this regime, the incident dislocation is at positions given by $0 < s_1 \leq r_c$. For this stage of the model, the evolution of the incident dislocation core into the cores of product dislocations must be captured. Hence, all dislocations involved are modeled as Peierls dislocations (Section 2.1.1). A general overview of this stage of the model is as follows. The position of the incoming dislocation, given by s_1, is taken as input. At each position, the CRSS $\tau^{\mathrm{II}}_{\mathrm{CRSS}}(s_1)$ is determined based on minimization of a Gibbs' free energy of the system involving continuum strain-energies and atomistic misfit energies of all dislocation cores. This formulation is motivated from the Generalized Peierls-Nabarro model developed in (Alkan et al., 2018a; Alkan and Sehitoglu, 2019; Foreman et al., 1951; Kroupa and Lejček, 1972; Lejček and Kroupa, 1976) for non-planar cores of slip dislocations in BCC materials, and adapted for the first time to the D-TB interaction.

2.1.3.1. Core descriptors (disregistry, dislocation density, and core-width) for dislocations in the D-TB reaction. From Table 1, it can be noted that there are 4 dislocation cores involved in each of the D-TB reactions, henceforth represented by the following serial numbers: (1) the core of incoming Shockley partial $\overrightarrow{b}_{LP}$, (2) the core of the incorporated twinning partial $\overrightarrow{b}_{TP}$, and two dislocation cores constituting the sessile stair-rod dislocation – (3) stair-rod Shockley partial $\overrightarrow{b}_{SR-SP}$ and (4) stair-rod twinning partial $\overrightarrow{b}_{SR-TP}$. The disregistry distribution and dislocation densities for each participating dislocation are given by the equations:

$$f_i(x) = \alpha_i b_i \left(\frac{1}{2} - \frac{1}{\pi}\tan^{-1}\left(\frac{x - s_i}{\xi_i}\right)\right); \rho_i(x) = -\frac{\alpha_i b_i \xi_i}{\pi\left((x - s_i)^2 + \xi_i^2\right)} \tag{2.8}$$

where $i = 1, 2, 3, 4$ represents each participating dislocation in the D-TB reaction, x_i represents the coordinate axis corresponding to each dislocation, s_i represents the position of the dislocations on their respective axes, b_i represent the Burgers vector magnitude, and ξ_i represent the core-width of the dislocations. The axes, positions and disregistry distributions are schematically represented in Fig.s 4 (a). Note that this form of the disregistry distribution is consistent with Eq. (2.3) and is chosen since the evolving disregistries and dislocation densities are directed towards the D-TB intersection, point O, as shown in Fig.s 4 (b, e). The pre-factors α_i capture the evolving state of each dislocation core between its initial state before the reaction, $\alpha_i = \alpha_i^{\mathrm{init.}}$, to its final state after the reaction $\alpha_i = \alpha_i^{\mathrm{final}}$(refer Fig. 4 (c, f)). The pre-factors are solved for in the model throughout the progression of core-evolution in the reaction, as elaborated later in this section. Note that $\{\alpha_i^{\mathrm{init.}}, \alpha_i^{\mathrm{final}}\}$ varies for each dislocation in the reaction, varying from $\alpha_1^{\mathrm{init.}} = 1 \rightarrow \alpha_1^{\mathrm{final}} = 0$ for the incoming leading partial $\overrightarrow{b}_{LP}$, $\alpha_2^{\mathrm{init.}} = 0 \rightarrow \alpha_2^{\mathrm{final}} = 1$ for the incorporated twinning partial $\overrightarrow{b}_{TP}$, and $\alpha_{3,4}^{\mathrm{init.}} = 0 \rightarrow \alpha_{3,4}^{\mathrm{final}} = \lambda_{3,4}$ for the stair-rod constituents (i.e. stair-rod Shockley partial, $\overrightarrow{b}_{SR-SP}$, and stair-rod twinning partial, $\overrightarrow{b}_{SR-TP}$), as partitioned in Table 1 and illustrated in Fig.s 4 (c, f).

Note that the disregistry within each core involves displacements only along the direction of the respective Burgers vectors of the participating dislocations. At the location of slip-twin intersection O, where all the evolving cores meet, it is unphysical to have all displacements accommodated unless the displacements are all zero. Thus, at O, the following condition needs to be satisfied:

$$\rho_i(x_i = 0) = 0 \tag{2.9}$$

However, this condition is too strong to implement numerically and a finite tolerance must be allowed. The reason being that for $\rho_i(x_i = 0) = 0$ to be satisfied exactly at O, we must have $s_i \rightarrow \infty$ due to the asymptotic nature of the dislocation density distribution (refer Fig. 4 (e) and Eq. (2.8)). Consequently, it leads to issues for numerical convergence in the model. Hence, a small non-zero tolerance is introduced instead, given by:

$$\rho_i(x_i = 0) = -\varepsilon_i b_i \tag{2.10}$$

where $\varepsilon_i = 0.05$ is chosen as the tolerance for all $i = 1, 2, 3, 4$. Note that the negative signs are from the choice of convention of the disregistry function (Eq. (2.8)). Having chosen this tolerance, the pre-factors α_i can be determined as a function of the position, s_i, and core-width of the dislocation, ξ_i, from Eq.s (2.8) and (2.10) as:

$$\alpha_i(s_i, \xi_i) = \frac{\varepsilon_i\left(s_i^2 + \xi_i^2\right)\pi}{\xi_i} \; (i = 1, 2, 3, 4) \tag{2.11}$$

Thus, any state of the dislocation cores during the reaction can be characterized given the parameters: $\{s_i, \xi_i\}$, $i = 1, 2, 3, 4$. The position of the incoming leading partial s_1 is taken as input, and incrementally reduced starting from $s_1 = r_c = 5b_{LP}$ to simulate the approach of the incoming leading partial. At each value of s_1, the remaining parameters $\{s_j, \xi_i\}$ (where $j = 2, 3, 4$ and $i = 1, 2, 3, 4$) are solved for, progressively revealing the evolution of the product dislocation cores. In solving for these parameters, a constraint must be enforced. This constraint is the conservation of the total Burgers vector, given by

$$\sum_{i=1}^{4} \overrightarrow{b}_i = \sum_{i=1}^{4} \left(\int_0^{s_j^{\max}} \widehat{b}_i \rho_i(x_i) dx_i \right) = \overrightarrow{b}_1 \tag{2.12}$$

Table 2
Elastic constants (in GPa) of the materials

Material	C_{11}	C_{12}	C_{44}	Ref.
Ni	261	151	132	(Gene and Herbert, 1971)
Cu	161.2	123.8	75.6	(Neighbours and Smith, 1954)
Pb	55.6	45.4	19.4	(Gene and Herbert, 1971)
Ag	131.5	97.3	51.1	(Gene and Herbert, 1971)
FeNiCoCrMn	221	152	165	(Alkan et al., 2018b)

Table 3
Anisotropic Parameters K_{ij} for Reaction I ($\times 10^2$ GPa)

Material	K_{11}	K_{22}	K_{33}	K_{44}	K_{12}	K_{23}	K_{13}	K_{14}	K_{24}	K_{34}
Ni	− 0.9466	− 0.8934	− 1.1458	− 1.3582	− 0.7651	1.1445	− 1.2092	− 1.4359	− 1.1951	1.1912
Cu	− 0.4738	− 0.4434	− 0.6309	− 0.7525	− 0.3483	0.6314	− 0.67	− 0.7973	− 0.66	0.6616
Pb	− 0.1278	− 0.1202	− 0.1772	− 0.2078	− 0.0913	0.1771	− 0.1891	− 0.22	− 0.1862	0.186
Ag	− 0.3639	− 0.3429	− 0.4781	− 0.5621	− 0.2746	0.4778	− 0.5035	− 0.5929	− 0.4973	0.4964
FeNiCoCrMn	− 0.931	− 0.8674	− 1.1458	− 1.4	− 0.7246	1.1424	− 1.2548	− 1.5052	− 1.2313	1.2212

where $\widehat{b}_i = \left(\frac{\overrightarrow{b}_i}{b_i}\right)$ (for $i = 1,2,3,4$) is the unit vector along the Burgers vector of each participating dislocation in the reaction. In other words, throughout the D-TB reaction, the net Burgers vector equals that of the incoming leading partial i.e. $\overrightarrow{b}_1$. As the cores evolve, the integrals in (2.12) are evaluated numerically, with the upper limit chosen as a large value $s_i^{\max} = 500b_{LP} \gg r_c$. The conserved Burgers vector magnitude b_1 of the leading partial is calculated as an integral of its dislocation density when the incoming partial is sufficiently far away from the TB, i.e. at $s_1 = 20b_{LP} \gg r_c$, given by:

$$b_1 = \int_0^{S_1^{\max}} \rho_1(x_1)_{s_1 = 20b_{LP}} dx_1 \tag{2.13}$$

It must be mentioned that the calculation in (2.13) results in $b_1 \approx b_{LP}$, i.e. a practical approximation of the Burgers vector magnitude of the leading partial. Only if the integral were calculated with the theoretical limits of $s_1 = \infty$ and $S_1^{\max} = \infty$, can we have the exact equality given by

$$b_1 = \int_0^{\infty} \rho_1(x_1)_{s_1 = \infty} dx_1 = b_{LP} \tag{2.14}$$

However, the integral in (2.14) is impractical to implement and leads to issues in numerical convergence during the progressive evolution of the dislocation cores at finite positions of the incoming leading partial, s_1. Thus, the calculation (2.13) is preferred and is correct for the model. Given the remaining state parameters $\{s_j, \xi_i\}$ ($j = 2,3,4$ and $i = 1,2,3,4$) and the constraint (2.12) specifying a set of admissible values for them, the solution procedure for the exact values during core-evolution is described below.

2.1.3.2. Solution Procedure. At each s_1, the total potential energy functional is computed for the system as a function of the state parameters $E_{\text{TOTAL}} = E_{\text{TOTAL}}(s_j, \xi_i, \sigma_a)$. This functional is a sum of the elastic strain energy of the individual dislocations and their mutual interaction, $E_{\text{ELASTIC}}(s_j, \xi_i)$, image interaction of all dislocations with the TB, $E_{\text{IMAGE}}(s_j, \xi_i)$, the atomistic energies of misfit within each of the dislocation cores, $E_{\text{MISFIT}}(s_j, \xi_i)$, and finally the work potential of the applied load on all dislocations, $-W(s_j, \xi_i, \sigma_a)$. The functional is given by the equation:

$$E_{\text{TOTAL}} = E_{\text{ELASTIC}} + E_{\text{IMAGE}} + E_{\text{MISFIT}} - W \tag{2.15}$$

The calculation of each of the summands in Eq. (2.15) is described below. The elastic energy is calculated as,

$$E_{\text{ELASTIC}} = \sum_{i=1}^{4} \sum_{j=i}^{4} \frac{K_{ij}}{2\pi} \int_t \int_x \rho_i(t)\rho_j(x) \ln \parallel x\widehat{s}_i - t\widehat{s}_j \parallel \, dxdt \tag{2.16}$$

where K_{ij} is an anisotropic elastic parameter that captures the elastic interaction energy between the $i^{\text{th}}$and the j^{th} dislocation involved in the reaction, and $\widehat{s}_i$ is the unit vector along the direction of increasing s_i (refer Fig. 4). Calculation of K_{ij} is detailed in Appendix C and depends on the anisotropic elastic constants (listed in Table 2), twin crystallography, and Burgers vector direction of participating dislocations. Hence, K_{ij} is dependent on the specific D-TB reaction and are listed in Tables 3, 4, 5 for the modeled slip-incorporation

Table 4
Anisotropic Parameters K_{ij} for Reaction II ($\times 10^2$ GPa).

Material	K_{11}	K_{22}	K_{33}	K_{44}	K_{12}	K_{23}	K_{13}	K_{14}	K_{24}	K_{34}
Ni	− 0.9466	− 1.1458	− 1.1458	− 0.9466	− 1.2092	1.2009	1.1509	− 0.9466	1.2539	− 1.1407
Cu	− 0.4738	− 0.6309	− 0.6309	− 0.4738	− 0.67	0.6449	0.6112	− 0.4738	0.6827	− 0.5987
Pb	− 0.1278	− 0.1772	− 0.1772	− 0.1279	− 0.1891	0.1813	0.1704	− 0.1278	0.1922	− 0.1673
Ag	− 0.3639	− 0.4781	− 0.4781	− 0.3639	− 0.5035	0.4865	0.4643	− 0.3639	0.5089	− 0.459
FeNiCoCrMn	− 0.931	− 1.1458	− 1.1458	− 0.931	− 1.2548	1.1797	1.0989	− 0.931	1.2663	− 1.0726

Table 5
Anisotropic Parameters K_{ij} for Reaction III ($\times 10^2$ GPa)

Material	K_{11}	K_{22}	K_{33}	K_{44}	K_{12}	K_{23}	K_{13}	K_{14}	K_{24}	K_{34}
Ni	− 0.9466	− 0.9257	− 1.1458	− 1.3582	− 0.8883	1.1805	1.1509	− 1.4763	1.1643	− 1.169
Cu	− 0.4738	− 0.4434	− 0.6309	− 0.7525	− 0.4068	0.6314	0.6112	− 0.7973	0.6213	− 0.6197
Pb	− 0.1278	− 0.1202	− 0.1772	− 0.2078	− 0.109	0.1771	0.1704	− 0.22	0.1733	− 0.1735
Ag	− 0.3639	− 0.3429	− 0.4781	− 0.5621	− 0.3164	0.4778	0.4643	− 0.5929	0.4706	− 0.4715
FeNiCoCrMn	− 0.931	− 0.8674	− 1.1458	− 1.4	− 0.8135	1.1424	1.0833	− 1.5052	1.1067	− 1.1168

Table 6
Prelogarithmic energy factors (in GPa) for reactions listed in Table 1

Material	E_1^0	E_1^∞	E_4^0	E_4^∞
Ni	7.8167	7.7237	10.9254	10.5535
Cu	3.7288	3.6709	5.9389	5.7074
Pb	1.0057	0.9931	1.6482	1.5978
Ag	2.8696	2.8357	4.4214	4.2857
FeNiCoCrMn	7.2599	7.1077	11.0277	10.4186

reactions I, II, and III respectively.

Determination of the correct K_{ij} is critical to determine the elastic energy E_{ELASTIC} accurately, particularly when the elastic constitution of the material is anisotropic as in all considered cases of this study. A common approximation from isotropic elasticity is to use the elastic shear modulus $\mu = C_{44}$ for all the interaction parameters K_{ij} (Hirth and Lothe, 1983). Such an approximation however cannot account for the mixed nature of the participating dislocations, the full elastic anisotropy of the material, or the varying strengths of elastic interaction between different dislocations (i.e. K_{ij} could strongly vary for different i and j). For instance, in reaction I in Ni, notice the significant variation in the magnitude of the anisotropic interaction parameters K_{ij} for different i and j (refer first row of Table 3), calculated by the proposed approach in this study (Appendix C). These magnitudes differ from the shear modulus C_{44} by over 50% of the modulus (refer Table 2), implying a proportionate difference in the elastic energy E_{ELASTIC}. In that regard, the isotropic approximation would lead to erroneous results and the anisotropic calculation proposed in this study is necessitated for correct calculation of the elastic energy.

The image interaction energy can also be evaluated in a similar manner as the elastic energy above. Only two dislocations, the incoming leading partial and the stair-rod Shockley partial, have an explicit energy of image interaction with the TB (the other dislocations are directly on the TB and have no image interaction energy). The image interaction energy is given by the expression:

$$E_{\text{IMAGE}} = \sum_{i\in\{1,4\}} \left(E_i^0 - E_i^\infty\right) \int_0^{s_i^{\max}} \rho_i(x)^2 \ln(x\sin\theta_i)dx \tag{2.17}$$

where θ_i is specified in Fig. 4 (a) and E_i^0 and E_i^∞ are pre-logarithmic energy factors (as defined in Section 2.1.1) corresponding to dislocations with unit Burgers vectors $\widehat{b}_i = \overrightarrow{b}_i/b_i$. As discussed in Section 2.1.1 and further in Appendix A, the pre-logarithmic factors E_i^0 and E_i^∞ capture the elastic strain energy of the i^{th} dislocation when it is on the TB ($s_i \to 0$) and when it is far away from the TB ($s_i \to \infty$) respectively. Consequently, the difference of these energy factors, as seen in Eq. (2.17), effectively captures the magnitude of elastic interaction energy with the TB. The calculation of the pre-logarithmic energy factors is deferred to Appendix A. They depend on the anisotropic elastic constants, the twin crystallography and the direction of the Burgers vector. It is sufficient to evaluate the pre-logarithmic factors for the unit Burgers vectors: $\widehat{b}_1 \| [2\bar{1}\bar{1}]_{\text{M}} = [\bar{2}\bar{1}1]_{\text{T}}$ and $\widehat{b}_4 \| [\bar{1}2\bar{1}]_{\text{T}}$. These two Burgers vectors correspond to the incoming Shockley partial and the stair-rod Shockley partial for all reactions I, II and III (refer Table 1). The computed pre-logarithmic factors, E_i^0 and E_i^∞, are listed in Table 6. To the best of our knowledge, such an explicit determination of these factors for image

interaction energies, in the presence of elastic anisotropy, has not been made in prior studies.

Next, the applied work is evaluated as:

$$W = \sum_{i=1}^{4} \int_{0}^{s_i^{\max}} \left(\left(\underline{\underline{\sigma_a}} \hat{n}_i \right) . \hat{b}_i \right) f_i(x) dx \tag{2.18}$$

where $\underline{\underline{\sigma_a}}$ is the applied stress tensor, $\hat{n}_i$ is the slip plane of the corresponding dislocation (making $\underline{\underline{\sigma_a}} \hat{n}_i . \hat{b}_i$ the Schmid factor), and $s_i^{\max}$, $\hat{b}_i$, $f_i(x)$ have been defined earlier. The applied stress tensor is determined from the loading direction $\hat{v}$ (Table 1), using the dyadic product i.e. $\underline{\underline{\sigma_a}} = \sigma_a(\hat{v} \otimes \hat{v})$.

Finally, the misfit energies of the dislocations, E_{MISFIT} , represent the atomistic energies of misfit/disregistry within their cores. To evaluate E_{MISFIT}, the generalized fault energies corresponding to the participating dislocations are required. In the D-TB reactions considered in this study, the Generalized Stacking Fault Energy (GSFE) curve for the Shockley partials - $\overrightarrow{b}_{LP}$ $(i=1)$ and $\overrightarrow{b}_{SR-SP}$ $(i=4)$, and the Generalized Planar Fault Energy (GPFE) curve for the twinning partials - $\overrightarrow{b}_{TP}$ $(i=2)$ and $\overrightarrow{b}_{SR-TP}$ $(i=3)$ are required. The respective fault energy curves can be well approximated by trigonometric functions (Chowdhury et al., 2014; Wang and Sehitoglu, 2013) given by the equations:

$$\begin{aligned}
\gamma_1(u) &= \begin{cases} \gamma_{\text{isf}} + \left(\frac{\gamma_{\text{us}} - \gamma_{\text{isf}}}{2}\right)\left(1 - \cos\left(\frac{2\pi u}{b_{LP}}\right)\right) & \text{for } 0 \le u \le \frac{b_{LP}}{2} \\ \frac{\gamma_{\text{us}}}{2}\left(1 - \cos\left(\frac{2\pi u}{b_{LP}}\right)\right) & \text{for } \frac{b_{LP}}{2} \le u \le b_{LP} \end{cases} \\
\gamma_2(u) &= \frac{\left(\gamma_{\text{ut}} - 2\gamma_{\text{tsf}}\right)}{2}\left(1 - \cos\left(\frac{2\pi u}{b_{TP}}\right)\right) \text{for } 0 \le u \le b_{TP} \\
\gamma_3(u) &= \frac{\left(\gamma_{\text{ut}} - 2\gamma_{\text{tsf}}\right)}{2}\left(1 - \cos\left(\frac{2\pi u}{b_{SR-TP}}\right)\right) \quad \text{for } 0 \le u \le b_{SR-TP} \\
\gamma_4(u) &= \begin{cases} \frac{\gamma_{\text{us}}}{2}\left(1 - \cos\left(\frac{2\pi u}{b_{SR-SP}}\right)\right) & \text{for } 0 \le u \le \frac{b_{SR-SP}}{2} \\ \gamma_{\text{isf}} + \left(\frac{\gamma_{\text{us}} - \gamma_{\text{isf}}}{2}\right)\left(1 - \cos\left(\frac{2\pi u}{b_{SR-SP}}\right)\right) & \text{for } \frac{b_{SR-SP}}{2} \le u \le b_{SR-SP} \end{cases}
\end{aligned} \tag{2.19}$$

Thus from Eq. (2.19), the critical fault energies involved in the D-TB reaction are the unstable stacking fault energy γ_{us}, stable intrinsic stacking fault energy γ_{isf}, the unstable twinning energy barrier γ_{ut}, and the twin boundary energy γ_{tsf}. These energies are listed in Table 6 for all materials in this study. The fault energies for Ni-based alloys were determined from additional Molecular Dynamics (MD) and Molecular Statics (MS) simulations in this study, discussed in Appendix D. Given the fault energy landscapes and the critical fault energies, the total misfit energy of the system is given by the equation:

$$E'_{\text{MISFIT}} = \sum_{n=1}^{4} \sum_{t=0}^{\infty} \gamma_i(f_i(ta'_i))a'_i \approx \sum_{n=1}^{4} \sum_{t=0}^{T_i^{\max}} \gamma_i(f_i(ta'_i))a'_i \tag{2.20}$$

where t is an integer varying from 0 to $T_i^{\max}$, $T_i^{\max} = \lceil S_i^{\max}/b \rceil$ is the smallest integer larger than $S_i^{\max}$, and a'_i represents periodicity in the lattice. The concept of a discrete periodicity is a key to determine the misfit energy. It has thus far been assumed to be the periodicity in atomic positions of the underlying crystal structure, normal to the dislocation line along the disregistry distribution (i.e. along directions of increasing x_i in Fig. 4). We assert that this is only true for the special case where the dislocation is of edge character and generalize for the case of mixed dislocations as are involved in the D-TB reactions. This is a significant and necessary modification. We state that the periodicity a' more generically corresponds to the periodicity in the energy landscape along the Burgers vector of the dislocation. This periodicity is the same as the magnitude of the Burgers vector of the dislocation itself. Hence, we have $a'_i = b_i$ for all the dislocations in this reaction.

Finally, the misfit energy of the intrinsic stacking fault trailing behind the leading partial must be excluded. This is because the $a/2\langle 011 \rangle$ extended dislocation is presumed to approach the TB without any change in the stacking fault length between its two $a/6\langle 112 \rangle$ partials, and only the leading partial interacts with the TB in the slip-incorporation D-TB reaction. Thus, Eq. (2.20) is modified as:

$$E_{\text{MISFIT}} = E'_{\text{MISFIT}} - \gamma_{\text{isf}}\left(S_1^{\max} - s_1\right) = \sum_{n=1}^{4} \sum_{t=0}^{T_i^{\max}} \gamma_i(f_i(tb_i))b_i - \gamma_{\text{isf}}\left(S_1^{\max} - s_1\right) \tag{2.21}$$

Now that all the summands in Eq. (2.15) have been determined, E_{TOTAL} can now be computed. The constraint of conservation of Burgers vector (Eq. (2.12)) is included through a vector of Lagrange multipliers $\overrightarrow{\mu} = (\mu_1, \mu_2, \mu_3)$, given by:

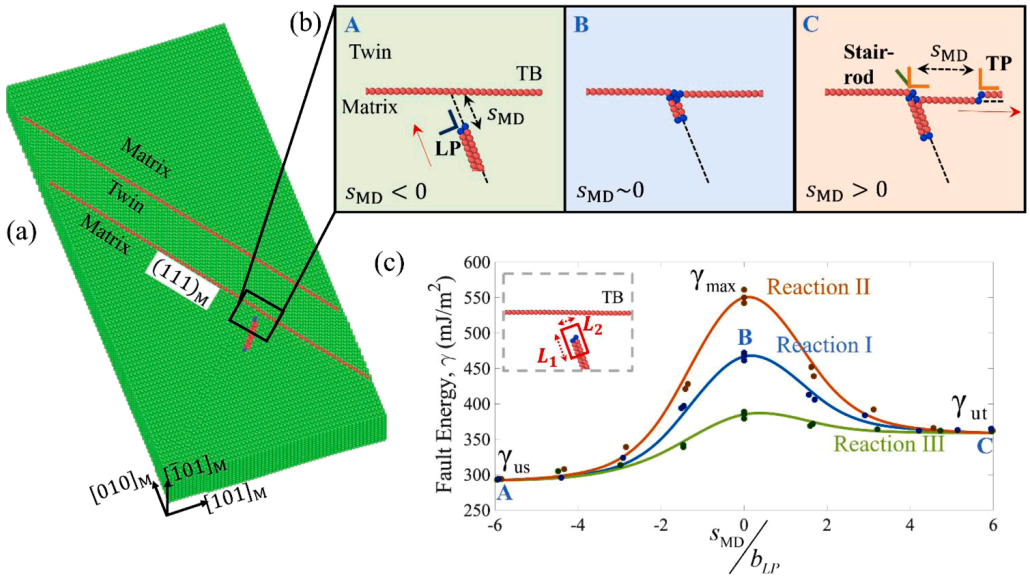

Fig. 5. Validation of EDC model through atomistic simulations: (a) Constructed crystal structure within the simulation supercell including a $(111)_M$ twin and an extended $a/2[110]_M$ dislocation dissociated into a leading partial $a/6[21\bar{1}]_M$ and trailing partial $a/6[121]_M$; atomistic simulation of D-TB reaction III is shown here (b) Under applied load, the leading partial approaches the TB and undergoes a slip-incorporation reaction leading to formation of a stair-rod dislocation on the TB and an incorporated twinning partial;(c) the fault energy signature γ traced in a small control volume (represented in the inset) around the cores of the incident and incorporated partials vary depending on the specific D-TB reaction; note that $\gamma = \gamma_{us}$ at point A corresponding to the incoming Shockley partial, and $\gamma = \gamma_{ut}$ at point B corresponding to the incorporated twinning partial, and the peak energy γ_{max} obtained from the simulations is used to calculate the critical stress τ^{MD}_{CRSS} for each reaction (fault energies sampled at 13 positions are shown by the data points in Fig. 5 (c), and a curve fit is shown)

$$E_{II} = E_{TOTAL} + \vec{\mu}.\left(\vec{b}_1 - \sum_{i=1}^{4}\left(\int_0^{s_i^{max}} \hat{b}_i \rho_i(x_i)dx_i\right)\right) \tag{2.22}$$

where E_{II} is the objective function to be minimized and E_{TOTAL}, $\hat{b}_i$, $\vec{b}_1$, $\rho_i(x)$, S_i^{max}, have been defined earlier. For a given position of the leading partial s_1, E_{II} is minimized with respect to each of the parameters $\{s_j, \xi_i, \mu_j\}$ (where $j = 2, 3, 4$ and $i = 1,2,3,4$) at a given applied load σ_a. This yields the following equations that can be solved for the aforementioned parameters.

$$\frac{\partial E_{II}}{\partial s_j} = 0\,;\ \frac{\partial E_{II}}{\partial \xi_i} = 0\,;\ \frac{\partial E_{II}}{\partial \mu_j} = 0 \tag{2.23}$$

This problem is solved using the minimization routine implemented in the function *fmincon* in MATLAB®. An energy-minimized state $\{s_j^0, \xi_i^0\}$, at a given s_1 and applied load σ_a^0, corresponds to a state of equilibrium for the dislocation cores at that position under the load σ_a^0. The purpose of the model is to determine the critical applied load $\sigma_a^{cr.}$ required to drive core-evolution in the D-TB reaction at the given position of the incoming leading partial, s_1. In other words, we want to determine the critical load $\sigma_a^{cr.}$, at a given s_1, when the system departs from equilibrium or is unable to find an energy-minimizing equilibrium state. To determine this load, we start from $\sigma_a = 0$ and increment the load in discrete steps. At each step, the energy-minimized state $\{s_j, \xi_i\}$ is determined. At the critical load, $\sigma_a = \sigma_a^{cr.}$, the system reaches an instability where either the minimum does not exist (i.e. no solution to (2.23) and solver runs into an infinite loop), or the minimizing state parameters are unphysical. The state of the evolved dislocation cores $\{s_j^{cr.}, \xi_i^{cr.}\}$, at this critical load is taken from the energy-minimized state from the previous load step. The occurrence of such an instability as a marker of critical applied load, has been previously suggested in early works on non-planar cores in BCC materials (Alkan and Sehitoglu, 2019; Kroupa and Lejček, 1972; Kroupa and Vítek, 1967) and is adapted for the EDC model as described above. The critical load is interpreted as a CRSS on the incident slip system, given by $\tau^{II}_{CRSS} = \left(\underline{\underline{\sigma_a^{cr.}}}\hat{n}_1\right)\hat{b}_1$ for stage 2 of the EDC model. Thus, by determining $\tau^{II}_{CRSS}(s_1)$ and $\{s_j^{cr.}, \xi_i^{cr.}\}$ at different s_1 values, the EDC model determines the critical stress for the D-TB reaction to occur and reveals the evolving cores during the reaction.

2.2. Atomistic Simulation of Dislocation Reactions

The results of the EDC model are validated against atomistic simulations of each D-TB reaction considered. Simulations are per-

formed in LAMMPS (Plimpton, 1995) with Ni as the study target, employing the interatomic potential developed in (Ren and Sehitoglu, 2016). The simulation supercell is constructed with the axes aligned with crystallographic directions of the matrix as follows: $x \parallel [101]_M$, $y \parallel [010]_M$ and $z \parallel [\bar{1}01]_M$. The box dimensions are chosen as $30L_{[101]} \times 90L_{[010]} \times 10L_{[\bar{1}01]}$, where $L_{[uvw]}$ represents one periodic distance along $[uvw]_M$ in the lattice. A 15-layer twinned region is introduced into the crystal structure, with the TB on a $(111)_M$ plane, as shown in Fig. 5. Periodic boundary conditions are enforced across the boundaries normal to the z-axis (i.e. xy bounding planes) while shrink-wrapped boundary conditions are enforced across the xz and yz bounding planes. At the shrink-wrapped boundaries, a thin layer of atoms with a thickness higher than the interatomic potentials's cutoff distance is specified. In this layer all atoms are constrained from moving in any direction, serving as the pristine twinned crystal structure bounding a mobile core region of the simulation box where the D-TB reaction is to be simulated. The $a/6\langle 112\rangle$ Shockley partials are introduced by first inserting a $a/2\langle 110\rangle$ full dislocation on a $\{111\}$ slip plane and then equilibrating the atomic structure to foster splitting of the full dislocation into two partials separated by a stacking fault. Thus, an extended $a/2[110]$ dislocation is inserted within the matrix on the $(1\bar{1}1)_M$ by enforcing the anisotropic elastic displacement field on the atomic structure. The constructed atomic structure is first relaxed using the conjugate gradient energy minimization. Subsequently, a low-temperature of 10 K is ascribed to the system by first initializing atomic velocities corresponding to this temperature and then executing a Molecular Dynamics (MD) run at this temperature for 1 pico-second (1000 simulation time steps of 1 femto-second each).

After both these equilibrating simulations, the extended dislocation splits to form two $a/6\langle 112\rangle$ Shockley partials, the leading partial of which is $\overrightarrow{b}_{LP} = a/6[21\bar{1}]_M$. Strain-controlled loading along $[010]_M$, $[1\bar{2}3]_M$, and $[11\bar{1}]_M$ crystal orientations are applied for the reactions I, II, and III respectively and velocity verlet time-integrator has been used to advance the dynamic time steps during deformation. OVITO (Stukowski, 2009) is utilized to visualize the results and the in-built dislocation analysis tool is used to confirm that the observed D-TB reactions match with the targeted reactions. As anticipated, under specified loading, the incident leading partial moves towards the TB and upon impact triggers the corresponding incorporation reactions.

2.2.1. Control Volume Approach (CV + PN)

Next, we determine the CRSS required for each D-TB reaction within a Molecular Dynamics (MD) framework. This study proposes a modified approach that tracks a local Control-Volume (CV) surrounding the dislocation cores in the simulation, combining with the Peierls-Nabarro (PN) model to determine the CRSS. Thereby this approach focuses on dislocation core-evolution in the simulations and overcomes the unduly high-stresses in MD due to strain-rate effect. The approach employed is motivated from (Chowdhury et al., 2013; Ezaz et al., 2011; Sangid et al., 2012) where the average potential energy of a small CV of atoms is tracked. This control volume is chosen to be a cuboid with a rectangular projection on the $(\bar{1}01)_M$ plane, with dimensions $L_1 \times L_2$ where $L_1 = 2d_{\{111\}}$ spans along the slip plane of the dislocation core, and $L_2 = d_{\{111\}}$ spans normal to the slip plane (refer inset in Fig. 5 (c)), where $d_{\{111\}}$ is one interplanar spacing of the $\{111\}$ slip plane. The size of the CV is chosen to be this small because only then does the energy obtained from the CV directly correspond to the unstable fault energy of the dislocation core without involving its strain-energy. It has been previously shown that only at such small sizes does the fault energy obtained from the CV approach exactly match the unstable fault energies obtained from the GSFE (Chowdhury et al., 2013). The third dimension along $[\bar{1}01]_M$, parallel to the direction of the dislocation line, spans the length of the simulation box in that direction. This control volume is tracked throughout the D-TB reaction, subsequently following the incorporated twinning partial after completion of the reaction. The average energy of this tracked volume corresponds to the unstable stacking fault energy γ_{us} when the leading partial is away from the TB. As it approaches the TB and the D-TB reaction is triggered, an elevated fault energy γ_{max} is observed until the value saturates to the unstable twinning energy γ_{ut} of the incorporated twinning partial. A positional coordinate s_{MD} is specified to characterize the state of the reaction (refer Fig. 5). During approach of the incident partial, the coordinate characterizes the position of the partial away from the TB taken along the direction of approach, and after completion of the reaction, the coordinate characterizes the position of the incorporated twinning partial (TP) away from the stair-rod taken along the TB. Snapshots of the simulated incorporated reactions are shown in Fig. 5 (b), showing the behavior of the tracked fault energy in the control volume and the corresponding positional coordinate.

The CRSS for the D-TB reactions are determined from the elevated fault energy γ_{max} as follows. The leading partial is considered to be a Peierls dislocation with the disregistry distribution given by equation:

$$f(x) = b_{LP}\left(\frac{1}{2} + \frac{1}{\pi}\tan^{-1}\frac{x}{\xi_{cr.}}\right) \tag{2.24}$$

where $\xi_{cr.}$ is the critical core-width of the partial predicted by the EDC model when τ^{II}_{CRSS} is maximum (i.e. core-width at peak stress of the D-TB reaction predicted by EDC model). The elevated fault energy γ_{max} is taken as the unstable fault energy of the incident leading partial. The fault energy curve for the dislocation is then given by:

$$\gamma_{MD}(u) = \begin{cases} \gamma_{isf} + \left(\dfrac{\gamma_{max} - \gamma_{isf}}{2}\right)\left(1 - \cos\left(\dfrac{2\pi u}{b_{LP}}\right)\right) & \text{for } 0 \le u \le \dfrac{b_{LP}}{2} \\ \dfrac{\gamma_{max}}{2}\left(1 - \cos\left(\dfrac{2\pi u}{b_{LP}}\right)\right) & \text{for } \dfrac{b_{LP}}{2} \le u \le b_{LP} \end{cases} \tag{2.25}$$

To determine the Peierls stress, the misfit energy of the partial is calculated, given by the equation:

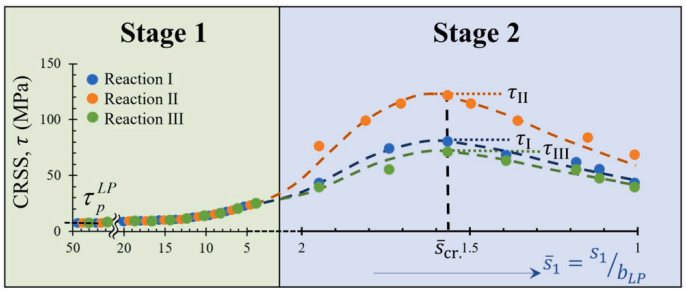

Fig. 6. CRSS predictions for each D-TB reaction listed in Table 1, are determined from the EDC model developed in this study; the CRSS on the incident slip system required to progress the D-TB reaction is predicted at varying positions of the incident leading partial, s_1; the peak CRSS on the incident slip system required for the reactions are respectively given by $(\tau_I, \tau_{II}, \tau_{III})$, observed at a critical position $s_1 = s_{cr.}$; the solid circles represent the predicted CRSS values from the EDC model, and the dashed trend-line is presented for convenience

$$E_{\text{MISFIT}-\text{MD}}(u) = \left(\sum_{m=-\text{M}_{\max}}^{\text{M}_{\max}} \gamma_{\text{MD}}(f(ma' - u))a' - \gamma_{\text{isf}}(\text{M}_{\max}a' + u) \right) \tag{2.26}$$

where $a' = b_{LP}$. A large value of $\text{M}_{\max} = 1000$ is chosen. Briefly, the misfit energy determined in this approach represents the barrier to be overcome by the incident partial to complete the D-TB reaction. The critical stress required to complete the D-TB reaction is then given by:

$$\tau_{\text{CRSS}}^{\text{MD}} = \max\left\{ \frac{1}{b_{LP}} \frac{d}{du} (E_{\text{MISFIT}-\text{MD}}(u)) \right\} \tag{2.27}$$

Thus, in summary, the critical stress $\tau_{\text{CRSS}}^{\text{MD}}$ is determined from the maximum gradient of the misfit energy$E_{\text{MISFIT}-\text{MD}}(u)$, with the misfit energy determined from the elevated unstable stacking fault energy $\gamma_{\max}$ within the CV during the reaction. The computed critical stress from MD, $\tau_{\text{CRSS}}^{\text{MD}}$, is compared against predictions of the EDC model. The results of the model and the atomistic validation are presented below. It is worth mentioning that the control volume approach is a robust framework within the state-of-the-art atomic-scale MD framework to analyze D-TB reactions. Yet it still requires careful analysis of a large set of evolving energies and atom positions for effective extraction of the CRSS, and is still reliant on the efficacy of the underlying interatomic potential. The EDC model has significant advantages to overcome these challenges as discussed below. The implications of the results are also discussed.

3. Results and Discussion

The results of the EDC model for the slip-incorporation reactions considered in Table 1, for the FCC material - Ni, are presented in Fig. 6. The critical applied stress is determined as the D-TB reaction progresses, with the progression characterized by the reducing magnitude of the incident partial's position s_1 with respect to the TB. The applied stress is resolved on the slip system of the incident partial to yield the CRSS for the incident dislocation. Note that the CRSS for all three reactions begin at the same value for large s_1 i.e. when the incident partial is away from the TB. This CRSS corresponds to the Peierls stress of the incident partial in the matrix, given by τ_p^{LP}, and is independent of the loading orientation. The CRSS starts elevating as the incident partial approaches due to a repulsive image stress from the TB. This is captured by stage 1 of the EDC model. Note that the CRSS-elevation in stage 1 is modest and nearly similar for all three D-TB reactions. When $s_1 < 5b_{LP}$, stage 2 of the EDC model is employed. In this stage, there is a distinct peak CRSS observed at a critical position $s_1 = s_{cr.}$, where the core-evolution from the incident partial to product dislocations is still ongoing. Further, the $s_{cr.}$ is not unique and can differ according to the reaction. The resulting CRSS-elevation is much higher than that observed in stage 1 and is significantly different across the three incorporation reactions.

Recall that the applied loading orientation $\underline{\underline{\sigma_a}} = \sigma_a(\widehat{v} \otimes \widehat{v})$, where $\widehat{v}$ is the direction of loading listed in Table 1, is distinct for each reaction. The critical applied stress $\sigma_a^{cr.}$ is interpreted as a resolved CRSS for the following reason: It is well-known that irrespective of the loading orientation $\widehat{v}$, the CRSS of a slip system in the matrix away from the TB, is a unique value (for FCC materials) primarily dependent on the underlying lattice friction (for given ambient conditions of temperature and pressure). The results of this study show that this uniqueness is broken under prevalence of D-TB reactions, as each D-TB reaction exhibits a distinct elevated CRSS. In other words, there is a more complex dependence of the critical stresses on the loading orientation that cannot be captured by a simple resolution of the applied load on a slip/twin system. And it is imperative to capture this dependence since the elevated CRSS values $(\tau_I, \tau_{II}, \tau_{III})$ for the D-TB reactions considered are at least 10-fold higher than τ_p^{LP}, critically affecting mechanical behavior in monotonic strain-hardening, cyclic fatigue etc. This dependence is captured by the EDC model. The predictions of the EDC model are validated against atomistic simulations that are currently one of, if not the best, state-of-the-art techniques to understand D-TB reactions. Results are presented in Table 8, showing excellent agreement.

The EDC model further clarifies the complete trajectory of the D-TB reaction in terms of how the core of the incident leading partial evolves into product dislocation cores. Taking reaction I as an example (refer Table 1), evolving core distributions of the reaction, for Ni, are presented in Fig. 7. Fig. 7 (a), 7 (b) and 7 (c) represent different states of progression of the reaction. The dislocation density

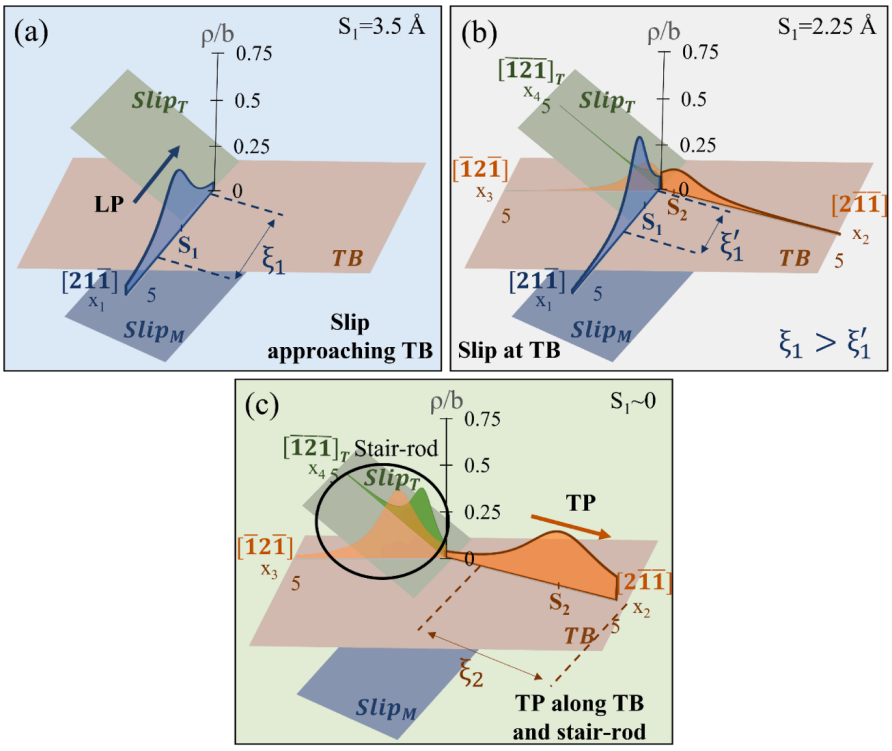

Fig. 7. Evolving core structures in D-TB reaction I in Ni: (a) Dislocation density distribution of the leading partial (LP) upon approach to the TB, the core-width of which is given by ξ_1 (b) Constriction of the incident core ($\xi_1' < \xi_1$) and redistribution to form product dislocations (c) Completion of the D-TB reaction marked by the formation of the complete twinning partial (TP) core and the stair-rod core structure (in the figure, slip_M refers to the slip plane of the incident partial in the matrix and slip_T refers to the slip plane within the twin)

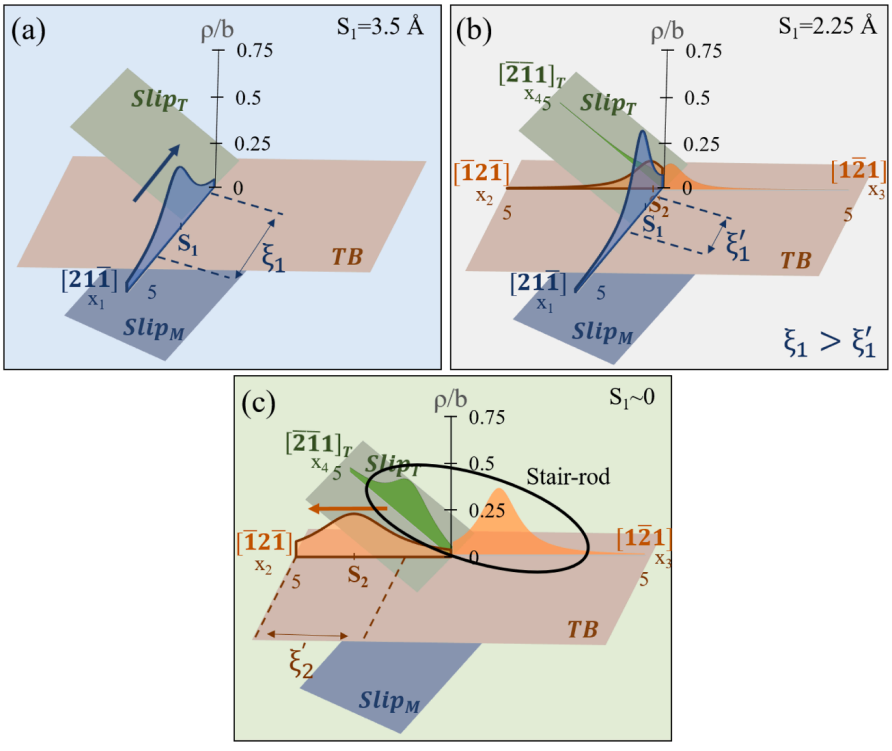

Fig. 8. Evolving core structures in D-TB reaction II in Ni: (a) Dislocation density distribution of the incident partial upon approach to the TB, the core-width of which is given by ξ_1 (b) Constriction of the incident core ($\xi_1' < \xi_1$) and redistribution to form product dislocations (c) Completion of the D-TB reaction marked by the formation of the complete twinning partial core and the stair-rod core structure (in the figure, slip_M refers to the slip plane of the incident partial in the matrix and slip_T refers to the slip plane within the twin)

Table 7
Fault Energies (in mJ/m^2 for FCC materials considered in this study: Stable intrinsic stacking fault energy γ_{isf}, unstable stacking fault energy γ_{us}, unstable twinning energy γ_{ut}, twin boundary energy γ_{tsf}

Material	γ_{us}	γ_{isf}	γ_{ut}	γ_{tsf}	Ref.
Ni	292	134	359	67	This study
Cu	180	41	200	20	(Kibey et al., 2007)
Pb	87	49	92	22	(Kibey et al., 2007)
Ag	133	18	143	9	(Kibey et al., 2007)
FeNiCoCrMn	439	8	538	7	(Alkan et al., 2018b)
Ni-10%Ti	220	126	266	64	This study
Ni-20%Ti	140	112	189	66	This study
Ni-3%Co	303	129	368	69.5	This study
Ni-10%Co	285	112	345	56	This study
Ni-20%Co	270	92	325	45	This study

Table 8
Comparison of twin interaction stresses (in MPa) obtained from both approaches and determined core-width of the incident leading partial at the critical configuration (ξ_{cr})

	Loading Orientation	Evolving Dislocation Core (EDC) Model (MPa)	Atomistic Simulations (CV + PN), τ_{CRSS}^{MD} (MPa)	ξ_{cr}(Å) (EDC)
Reaction I, τ_I	$[010]$	79	74	1.13
Reaction II, τ_{II}	$[1\bar{2}3]$	121	116	1.02
Reaction III, τ_{III}	$[11\bar{1}]$	68	62	1.15

distribution for the incident leading partial is plotted in Fig. 7(a). The core of the leading partial constricts $\xi_1' < \xi_1$ (Fig. 7 (b)) before redistributing to form the cores of the product dislocations. This constriction of the core explains the elevation of CRSS in stage 2 of the model as a narrower core leads corresponds to higher friction stress (Hirth and Lothe, 1983; Schoeck, 2002). It is worth emphasizing that such a constriction is characteristic of stage 2 and completely absent in the image-interaction regime of stage 1. In stage 1, the image-interaction of the incident partial with the TB is purely elastic and does not affect the core-width. In stage 2 however, the core-width changes are far more significant. And these changes are driven by a coupled influence of misfit energies in the evolving cores and elastic energies of interaction between the cores at close proximity to each other. This also explains the higher elevations in CRSS realized in stage 2 as compared to stage 1 because the CRSS is most sensitive to the core-width of the dislocation (Hirth and Lothe, 1983). The trajectory of evolving cores for reaction 2 is also shown in Fig. 8. Note that although the stair-rod dislocations in both reactions are composed of a Shockley partial core and a twinning partial's core, their relative orientations and the Burgers vectors are both different. Both these factors are involved in dictating the resulting CRSS elevation and is sufficiently captured by the EDC model. And although out of scope for the present study, it would be a worthwhile pursuit to further compare the predicted core-evolutions with predictions from atomic-scale simulations following the works of (Wang et al., 2012).

The capacity of the EDC model to predict critical stresses throughout reaction-progression arises from the model of the core-structure of sessile dislocations in the reaction, namely the stair-rod dislocations. As mentioned before in Section 1, there is currently no understanding of the core-structure of such sessile dislocations, to the best of the authors' knowledge, and it is the authors' opinion that this void is fundamentally responsible for the absence of analytical models for D-TB reactions. The EDC model forwards a rigorous derivation of the core-structure, for the first time in literature. This proposition is based on the fact that the underlying crystal structure (in this case, FCC) has certain preferred crystallographic slip/twin systems where dislocation disregistries prefer to distribute, exhibiting low atomistic misfit energy. Thus, any dislocation within the system will try to minimize its atomistic misfit energy by havings its core of disregistry distribute on these specific systems within the material. For instance, in FCC, this system is given by the $\{111\}$ family of planes, preferably admitting disregistries along the $\langle 112\rangle$ direction. The most preferred slip and twin system for FCC is the $\{111\}\langle 112\rangle$ system, with the Burgers vector of slip and twinning both of type $a/6\langle 112\rangle$. Now for a non-conventional Burgers vector, such as the $a/3\langle 010\rangle$ stair-rod in reaction I, it is plausible that the disregistry will prefer redistributing along $\{111\}\langle 112\rangle$ systems, with two or more such systems together forming the net core structure. This is precisely the basis behind the core decomposition in Table 1, eventually captured by the model as shown in Fig.s 7 and 8. For the stair-rods modeled, the decomposition specified in Table 1 is unique, and no other decomposition combines to give the final Burgers vector of the stair-rod dislocations. Ultimately, the success of this key modeling hypothesis can be evidenced from the agreement between CRSS predictions for the reactions and those obtained from atomistic simulations. It will be shown later that the EDC predictions agree with experiments on a distinct material system, further corroborating the success of this hypothesis and consequently of the model itself.

The efficacy of the model is illustrated by applying it to other FCC materials, also exhibiting its utility for exploration of next-generation alloys and ab initio materials design in general. We first focused on the effect of alloying elements Titanium (Ti) and Cobalt (Co) on the critical CRSS for D-TB reactions in Ni. Fault energetics of the considered alloy compositions are unavailable in the literature and were computed by the authors using molecular statics (MS), as described in Appendix D, and listed in Table 7. The elastic constants are assumed to be the same as that of Ni, primarily to study the impact of changed fault energetics brought about by alloying. The CRSS predictions from the EDC model, for the D-TB reactions I, II and III are plotted against the fault energy signatures as shown in

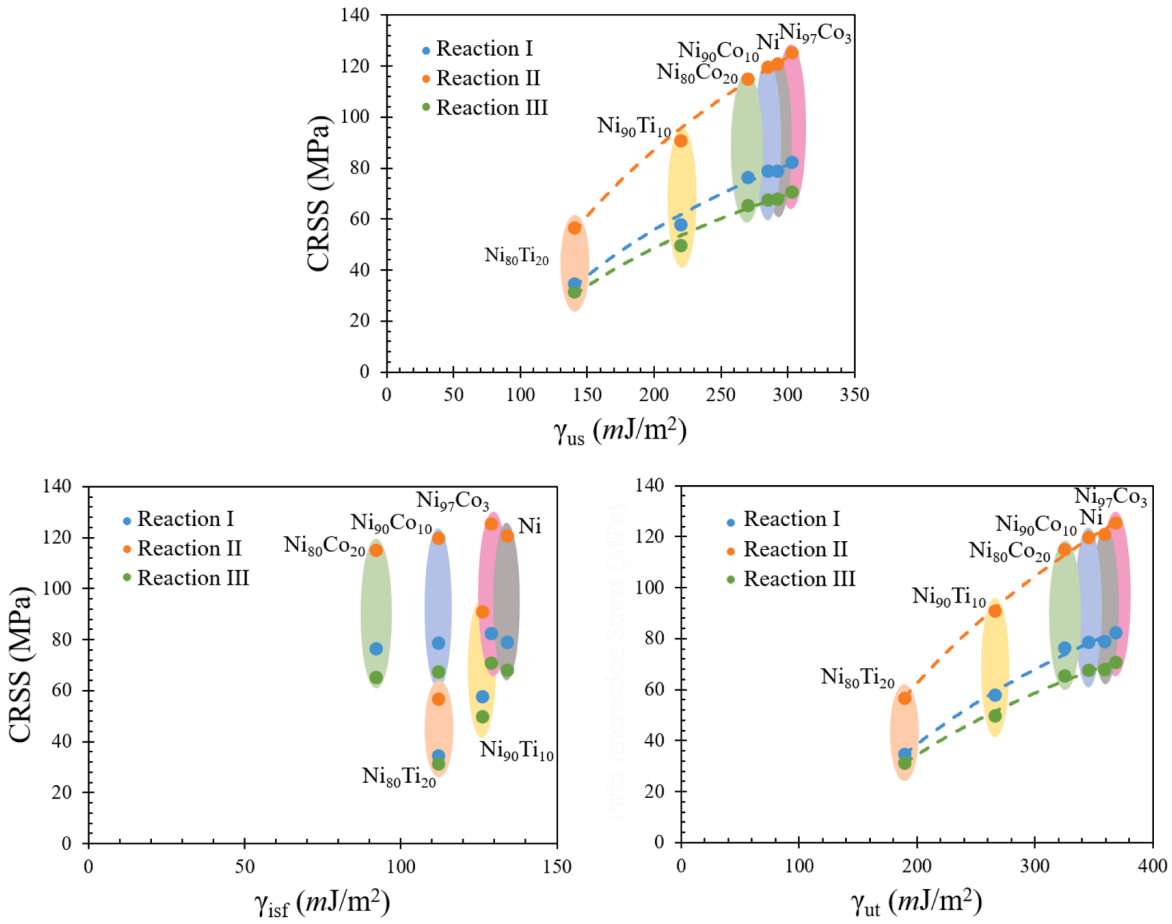

Fig. 9. EDC model applied to Ni-Ti and Ni-Co alloys; results are plotted against standard fault energy signatures in FCC materials, revealing a strongly positive correlation between the predicted CRSS for the D-TB reactions with the unstable stacking fault energy (γ_{us}) and unstable twinning energy (γ_{ut}); poor correlation is observed against the intrinsic stable stacking fault energy (γ_{isf})

Fig. 9. These results reveal the critical dependence of the CRSS on the unstable fault energies (unstable stacking fault energy, γ_{us}, and unstable twinning energy, γ_{ut}) for the first time in literature. Furthermore, it is shown that the commonly quoted intrinsic stacking fault energy γ_{isf}, although a good indicator of twinnability (Tadmor and Bernstein, 2004; Venables, 1961, 1964), is poorly correlated with the critical stresses of D-TB interaction. The implications of these dependencies are exemplified in the predictions for the Ni-Ti system, where the unstable fault energy signatures γ_{us} and γ_{ut} reduce far more sensitively with Ti concentration as compared to γ_{isf}, ultimately reflecting in a significant reduction of the CRSS for all 3 D-TB reactions considered. However, it must also be emphasized that an enhanced twinnability (due to lower γ_{isf}) impacts the mechanical behavior by extrinsically introducing additional twin barriers to dislocation slip, although intrinsically it has a modest effect on the D-TB critical stress itself.

We further extend the application of the EDC model to other FCC materials beyond Ni-based alloys, for the same reactions considered thus far. The same correlation between the underlying fault energetics and the predicted CRSS values are reiterated, as shown in Fig. 10. Note that the developed analytical framework is capable of modeling complex alloys such as the multi-component High Entropy Alloy (HEA) FeNiCoCrMn, for which reliable interatomic potentials are yet unavailable. While this would pose a challenge to study D-TB reactions within atomistic simulation frameworks, the EDC model is not limited by it as it relies on no empiricism at all. The success of the framework is rooted in the capacity to model atomic interactions of both elastic (recoverable stretching of atomic bonds) and inelastic (irrecoverable bond rearrangements) nature within the evolving dislocation cores. Thus, the model only relies on fundamental properties corresponding to each interaction, respectively the elastic constants and the fault energetics, ultimately dictating the predicted CRSS. The introduction of such a model is particularly important for the modern field of HEAs because the prevalence of high strain-hardening arising from slip-twin and twin-twin reactions has long been known but yet to be analyzed from an ab initio standpoint.

We further explore the versatility of the model by applying to several other incorporation reactions (listed in Table 9) in the FeNiCoCrMn system. The material elastic constants and fault energies material are listed in Tables 2 and 7 respectively, with the additional E and K constants calculated and listed in Tables 6 and 10 respectively. These reactions consider various stair-rod dislocations (with varying non-conventional Burgers vectors) that exhibit distinct core decompositions. For instance, in reaction V, the stair-rod dislocation $a/6[32\bar{3}]$ can only be described as a combination of the incident leading partial's core and a twinning partial on the TB. Note that this stair-rod decomposition implies the incident partial is halted at the TB, and thereby stops the trailing partial behind

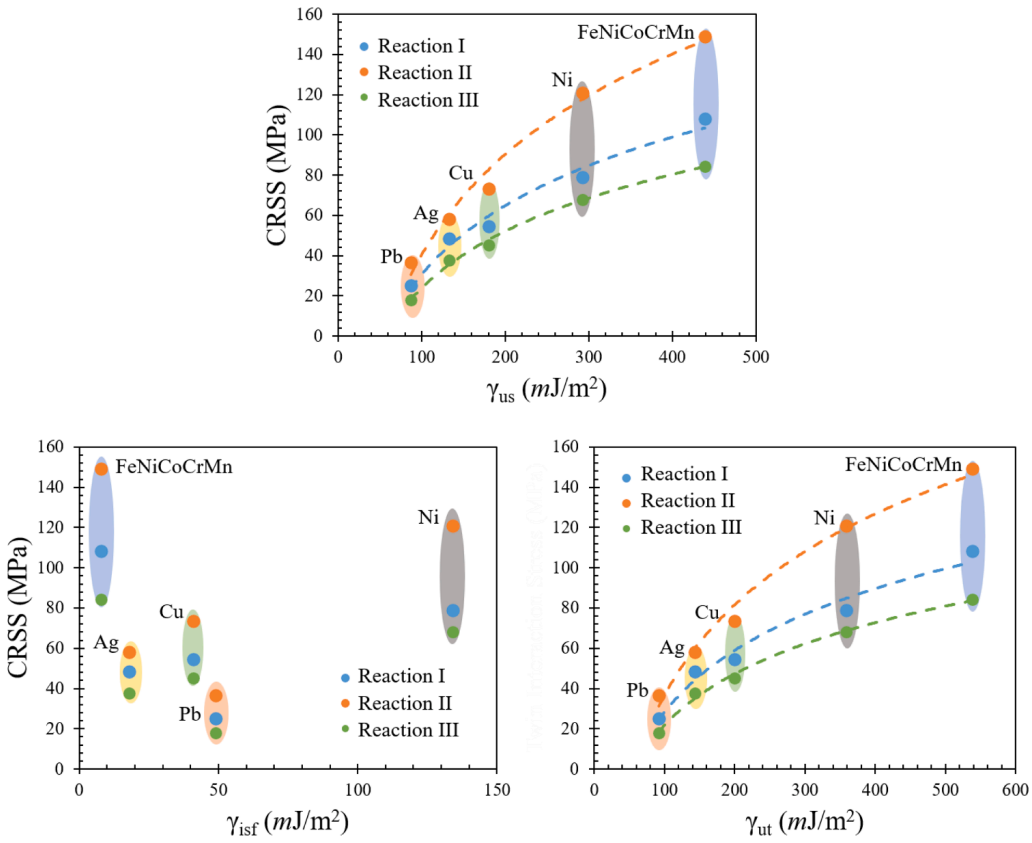

Fig. 10. EDC model applied to FCC materials: Pb, Ag, Cu, Ni and High Entropy Alloy (HEA) FeNiCoCrMn; results are plotted against standard fault energy signatures in FCC materials, revealing a strongly positive correlation between the predicted CRSS for the D-TB reactions with the unstable stacking fault energy (γ_{us}) and unstable twinning energy (γ_{ut}); poor correlation is observed against the intrinsic stable stacking fault energy (γ_{isf})

Table 9
Additional D-TB reactions considered in this study.

Loading Direction	Reaction #	Reaction
$[21\bar{2}]_M$	IV	$\frac{a}{6}[12\bar{1}]_M \rightarrow \frac{a}{6}[\bar{1}21]_M + \frac{a}{3}[10\bar{1}]_M$ *partial* *partial* *Shockley* *Twinning* *Stair − rod*
$[\bar{2}21]_M$	V	$\frac{a}{6}[21\bar{1}]_M \rightarrow \frac{a}{6}[\bar{1}\bar{1}2]_M + \frac{a}{6}[32\bar{3}]_M$ *partial* *partial* *Shockley* *Twinning* *Stair − rod*
$[\bar{2}13]_M$	VI	$\frac{a}{6}[12\bar{1}]_M \rightarrow \frac{a}{6}[\bar{1}\bar{1}2]_M + \frac{a}{6}[231]_M$ *partial* *partial* *Shockley* *Twinning* *Stair − rod*
$[31\bar{2}]_M$	VII	$\frac{a}{6}[12\bar{1}]_M \rightarrow \frac{a}{6}[\bar{2}1\bar{1}]_M + \frac{a}{6}[310]_M$ *partial* *partial* *Shockley* *Twinning* *Stair − rod*
$[010]_M$	VIII	$\frac{a}{6}[\bar{1}2\bar{1}]_M \rightarrow \frac{a}{6}[1\bar{2}\bar{1}]_M + \frac{a}{3}[\bar{1}00]_M$ *partial* *partial* *Shockley* *Twinning* *Stair − rod*
$[31\bar{2}]_M$	IX	$\frac{a}{6}[12\bar{1}]_M \rightarrow \frac{a}{6}[1\bar{2}\bar{1}]_M + \frac{a}{6}[040]_M$ *partial* *partial* *Shockley* *Twinning* *Stair − rod*

it. Such an incorporation reaction implies a slip-blockage as both partials are blocked by the TB. Thus, this study proposes a clarifying reason for blockage in context of the stair-rod core structures that form during the incorporation D-TB reaction. Furthermore, the core-structures associated with the reaction are shown in Fig. 11, for FeNiCoCrMn, revealing a highly constricted core and consequently a much elevated CRSS. The high CRSS value is further indicative of the tendency for slip-blockage associated with the reaction.

We further validate the physical fidelity of predictions from the EDC model by comparison with recent experimental data on the HEA FeNiCoCrMn. In refs. (Bönisch et al., 2018; Sidharth et al., 2020a), the strain-hardening behavior of the HEA was experimentally characterized (at low strain-rates and low-to-ambient temperature), noting the point of onset of slip-twin interactions based on Digital Image Correlation (DIC) and more precisely from the location of an inflection point on the strain-hardening region (of the stress-strain curve) where there is a distinct increase in slope. The corresponding D-TB reactions were also established. The experimental CRSS was

Table 10
Anisotropic Parameters (K) for FeNiCoCrMn Reactions (in $\times 10^2$GPa) for D-TB reactions in Table 9 (note that depending on the stair-rod decomposition in the reactions, there can be only 3 dislocation cores involved i.e. $i = 1, 2, 3$ instead of 4, reducing the number of K factors required in the model, as is the case for all reactions except reaction VIII below)

Reaction #	K_{11}	K_{22}	K_{33}	K_{44}	K_{12}	K_{23}	K_{13}	K_{14}	K_{24}	K_{34}
IV	− 1.3691	− 0.8674	− 0.8674	-	− 1.7706	1.0762	1.7304	-	-	-
V	− 0.931	− 0.8674	− 0.8674	-	0.7792	0.8466	− 0.8135	-	-	-
VI	− 1.3691	− 0.8674	− 0.8674	-	2.2503	1.3588	− 2.3076	-	-	-
VII	− 1.3691	− 1.1458	− 1.1458	-	− 1.2037	1.2072	1.2403	-	-	-
VIII	− 0.931	− 0.8674	− 1.1458	− 1.4008	− 1.3616	0.9089	− 1.8809	− 1.2844	− 2.2663	1.382
IX	− 1.3691	− 0.8674	− 0.8674	-	1.7304	1.0762	− 1.7706	-	-	-

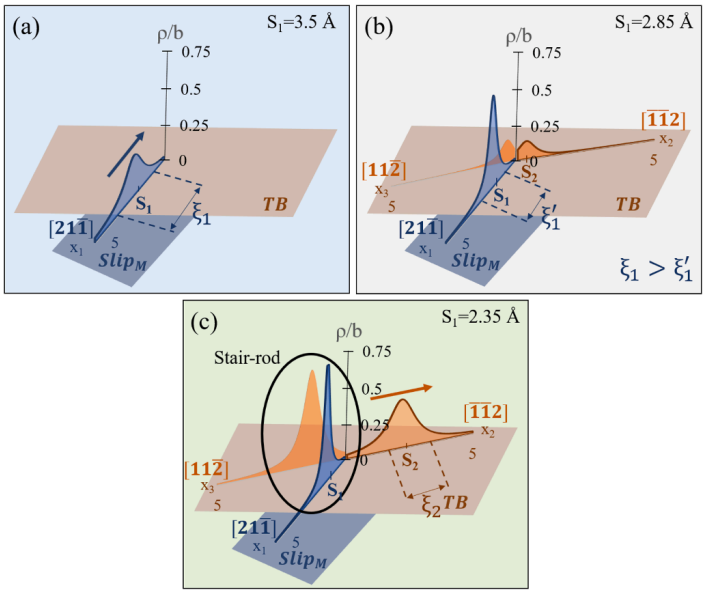

Fig. 11. Evolving core structures in D-TB reaction V in FeNiCoCrMn: (a) Dislocation density distribution of the incident partial upon approach to the TB, the core-width of which is given by ξ_1 (b) Constriction of the incident core ($\xi_1' < \xi_1$) and redistribution to form product dislocations (c) Completion of the D-TB reaction marked by the formation of the complete twinning partial core and the stair-rod core structure (note the composing cores of the stair-rod are from the incident Shockley partial and a twinning partial on the TB)

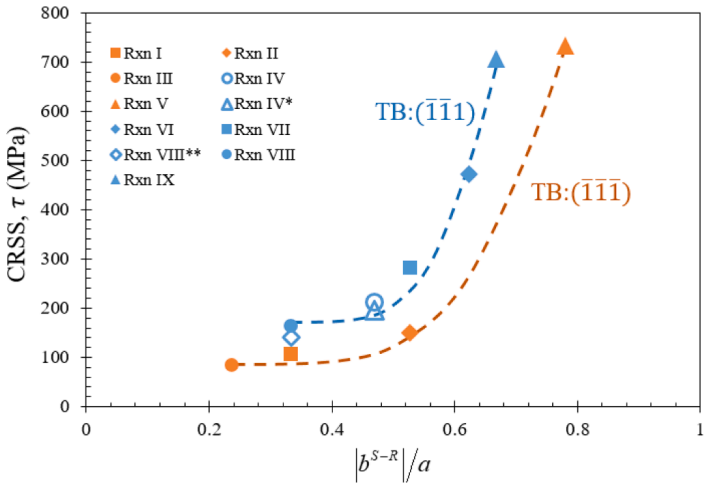

Fig. 12. CRSS for nine D-TB reactions studied on two different TBs are plotted against the magnitude of the sessile stair-rod dislocation in FeNiCoCrMn (*Experimental data from ref. (Bönisch et al., 2018); ** Experimental data from Ref. (Sidharth et al., 2020a))

obtained by applying the Schmid factor to the measured axial stress at the location of slip/twin interaction. The EDC model was applied to the corresponding D-TB reactions, on the respective TB observed, and the predicted CRSS values were compared against experiment (marked by * and **), showing good agreement, as shown in Fig. 12. At conditions of high strain-rates and/or high-temperature, the CRSS predictions of the EDC model would still offer a reliable baseline that can be further modified through an Arrhenius expression. The reader is referred to (Argon, 2007; Kocks et al., 1975) for a more detailed exposition on this topic. The predicted CRSS values are plotted against the residual Burgers vector magnitude, which in this case is the magnitude of the stair-rod dislocation's Burgers vector, validating the strongly positive non-linear correlation between the CRSS and $|b_{S-R}|$ formerly proposed in earlier studies (Abuzaid et al., 2012; Bönisch et al., 2018; Lee et al., 1989; Wu et al., 2018). The agreement with experimental results and with the atomistic simulations as shown before both validate the efficacy of the EDC model proposed in this study.

In summary, this study forwards an analytical framework capable of reliably predicting the critical stresses for D-TB reactions without any empiricism. While the current study focused on slip-incorporation reactions, we assert that the framework can be extended to study reactions of any type such as slip-transmission, multiplication, or even those involving an incident full-dislocation instead of an incident partial (Ezaz et al., 2011). For instance, to study a different type of D-TB reaction for the same material system and twin crystallography, the major changes required would be determination of the Burgers vectors involved, calculation of anisotropic interaction parameters, the number of disregistry cores and, the respective fault energy curves (γ_{us}, γ_{ut}, γ_{isf}), all of which are modifiable inputs into the same developed analytical framework. A change in the material system and twin crystallography can also be accommodated by appropriate changes in the material properties (fault energies and elastic constants) and the global coordinate system $\hat{e}_1 - \hat{e}_2 - \hat{e}_3$ in which the framework is developed (Fig. 2). Thus, the proposed framework can be adapted for other material systems such as HCP metals and alloys where D-TB reactions are widely prevalent and significantly influence mechanical response (Bacon and Vitek, 2002; Chen et al., 2019; Dang et al., 2021; Gong et al., 2018; Li et al., 2018; Serra and Bacon, 1996; Serra et al., 2002; Serra et al., 1991; Wang et al., 2014). Further, the framework also offers a foundation to analyze Dislocation-Grain Boundary (GB) interactions, capable of modeling the evolution of dislocation cores of the participating slip systems, provided the atomistic energy of the GB during the reaction is adequately determined and incorporated into the formalism (Kacher et al., 2014).

Ultimately, a prediction of the critical stresses for the D-TB reactions offers the capacity to quantify mechanical behaviors such as strain-hardening and fatigue initiation thresholds, both of which are strongly affected by D-TB interactions (Alkan and Sehitoglu, 2017). Even the scenarios of dislocation-absorption as recently revealed in HCP materials (Chen et al., 2019) can be approached using the proposed framework. EDC predictions can also serve as a useful metric to quantify Hall-Petch and inverse Hall-Petch effects in nanotwinned materials, by modeling the CRSS change due to repulsive or attractive interactions with TBs (Beyerlein and Tomé, 2008; Carlton and Ferreira, 2007; Gu et al., 2014b; Proust et al., 2009). The dependence of these behaviors on the orientation of the applied load and the underlying microstructure (i.e. the matrix-twin crystallography, the specific TB plane involved) can also be predictively explored preceding experimentation. Finally, the developed EDC model can be applied to several materials and alloys, including hypothetical materials compositions in materials design, useful for the exploration of next-generation materials with unprecedented mechanical properties.

4. Conclusions

In conclusion, this study forwards a new analytical framework, named the Evolving Dislocation Cores (EDC) model, to study Dislocation – Twin Boundary (D-TB) reactions and predict critical stresses for these reactions without empiricism. This is the first model of its kind to the best of the authors' knowledge. The following novel contributions are also forwarded:

a The model is versatile and can be adapted to distinct D-TB reactions. Critical stresses for 9 distinct slip-incorporation reactions have been predicted and good agreement of model-predicted stresses with atomistic simulations and experiments have been shown. The adaptation of the model for a different type of D-TB reaction (other than slip-incorporation) has been discussed, asserting the model's applicability with few straightforward modifications. The EDC model agrees with results from CV+PN approach based on MD and is further not limited by strain-rate effects or the fidelity of the MD potential which is a huge advantage.

b The EDC model successfully avoids the singularity of the elastic image interaction forces by duly considering the finite cores of the dislocations and the corresponding atomistic misfit energies within them. While the necessity of such considerations has been emphasized before and modeled for cross-slip of screw dislocations across TBs, this is the first time to the best of the authors' knowledge that such a model has been developed for a D-TB reaction involving multiple participating dislocations including an incident partial of mixed character and with sessile dislocations such as stair-rods.

c The developed model is devoid of any empiricism and relies on fundamental material properties, namely the elastic constants and fault energetics. Both properties can be reliably determined from ab initio predictive methods, such as Density Functional Theory (DFT), or experimental measurements. With this capability, the model can easily be applied to several materials as demonstrated in this study, and even for hypothetical material compositions considered during materials design. Thus, the proposed framework removes dependencies on empirical interatomic potentials or other empirical parameters necessitated by atomistic or Dislocation-Dynamics simulations. Further, the framework affords the opportunity for controlled study of the dependence of predicted critical stresses on underlying fault energies and elastic constants.

d A rigorous determination of the core-structure (core-widths) of complex sessile dislocations such as stair-rod dislocations are proposed for the first time in literature. A plausible decomposition of the non-conventional Burgers vectors of these sessile dislocations into a linear combination of preferred Burgers vectors on preferred slip systems of the underlying crystal structure is

proposed. The plausibility and efficacy of the proposed decomposition is validated by the agreement of critical stress predictions with atomistic simulations and experiments.

Author Statement

Orcun Koray Celebi: Methodology, Investigation, Software, Formal analysis, Validation, Writing – Original Draft, Writing – Review & Editing, Visualization; **Ahmed Sameer Khan Mohammed:** Conceptualization, Methodology, Software, Investigation, Writing – Original Draft, Writing – Review & Editing, Supervision; **Jessica A. Krogstad**: Supervision, Investigation, Project administration, Funding acquisition**; Huseyin Sehitoglu:** Conceptualization, Investigation, Supervision, Project administration, Funding acquisition, Writing – Review & Editing

Declaration of Competing Interest

The authors declare that they have no known competing financial interests or personal relationships that could have appeared to influence the work reported in this paper.

Acknowledgement

We note that O. K. Celebi and A. S. K. Mohammed contributed equally to this paper. The work is supported by the National Science Foundation (NSF) under award number CMMI-1761189, and partially by CMMI-2125821, which is gratefully acknowledged. The use of the Illinois Campus Cluster, a computing resource that is operated by the Illinois Campus Cluster Program (ICCP) in conjunction with the National Center for Supercomputing Applications (NCSA) and which is supported by funds from the University of Illinois at Urbana-Champaign, is also gratefully acknowledged.

Appendix A. Determining pre-logarithmic factors of image interaction energy: E^{∞} and E^{0}

The pre-logarithmic energy factors for anisotropic continuum media are determined using the Eshelby-Stroh formalism (Eshelby et al., 1953; Stroh, 1958). In this formalism, the displacement fields of dislocations, either in homogeneous anisotropic medium or on an interface between two anisotropic media are described by a set of complex constants. We first define the coordinate system given by the triad of vectors $\hat{m} - \hat{n} - \hat{t}$, where $\hat{n}$ is normal to the plane of disregistry of the dislocation, $\hat{m}$ lies on the plane of disregistry pointing away from disregistered side of the dislocation and $\hat{t} = \hat{m} \times \hat{n}$ (refer Fig. A1 (a)). The elastic constants for the matrix and the twin, in this coordinate system, are represented by C^1_{ijlm} and C^2_{ijlm} respectively. The reader is referred to (Bacon et al., 1980; Barnett and Lothe, 1974) for a more detailed exposition of the Eshelby-Stroh formalism and derivation of analytical expressions for the pre-logarithmic factors. In brief, sufficient for the purposes of the study, the Eshelby-Stroh constants $(p^1_\alpha, A^1_{k\alpha})$, $\alpha = 1, 2, 3 \ldots 6$ and $k = 1, 2, 3$ are determined by solving the equations:

$$C^1_{ijkm}\left(m_i + p^1_\alpha n_i\right)\left(m_m + p^1_\alpha n_m\right)A^1_{k\alpha} = 0 \tag{A.1}$$

$$\| \left(C^1_{ijkm}\left(m_i + p^1_\alpha n_i\right)\left(m_m + p^1_\alpha n_m\right)\right) \| = 0 \tag{A.2}$$

where the Einstein summation convention is followed in the indicial notations above and henceforth. The components of the vectors

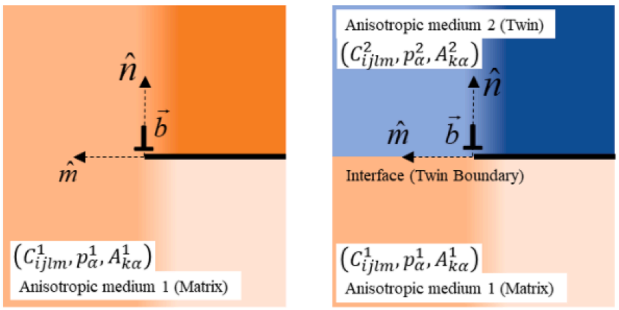

Fig. A1. Coordinate triad for Eshelby-Stroh formalism used to calculate the pre-logarithmic energy factors for image interaction energy; $\vec{b}$ is the Burgers vector of the dislocation, the thick line represents the plane of disregistry of the dislocation, $\hat{n}$ represents the normal to this plane and $\hat{m}$ lies on the plane of disregistry pointing away from the disregistered side; (a) $\hat{n}$ is normal to the slip plane, C^1_{ijlm} represents the elastic constants tensor for anisotropic medium 1, and $(p^1_\alpha, A^1_{k\alpha})$ are the Eshelby-Stroh constants for the medium (the matrix) (b) C^2_{ijlm} represents the elastic constants tensor for anisotropic medium 2 (the twin), and $(p^2_\alpha, A^2_{k\alpha})$ are the Eshelby-Stroh constants for the medium

and matrices are arranged following the convention

$$\begin{aligned} p_{\alpha+3} &= \overline{p}_{\alpha} \\ A_{k,\alpha+3} &= \overline{A}_{k\alpha} \end{aligned} \tag{A.3}$$

for $\alpha = 1,2,3$, where the bar on the RHS represents the complex conjugate. The normal vector $\hat{n}$ is the normal to the slip plane $(\overline{1}1\overline{1})_{\mathrm{M}}$ and $\hat{m}$ is chosen parallel to $[121]_{\mathrm{M}}$ (direction of increasing x_1 in Fig. 4).

As derived in ref. (Stroh, 1958), the pre-logarithmic factorE^{∞} is given by:

$$E^{\infty} = \frac{B_{mn} d_m d_n}{4\pi} \tag{A.4}$$

where d_i is obtained as

$$d_m = \left(B^{-1}\right)_{mn} b_n \tag{A.5}$$

given the Burgers vector $\overrightarrow{b}$ of the dislocation. And B_{mn} is determined as,

$$B_{mn} = -\frac{1}{2i} \sum_{\alpha=1}^{3} \left(A^1_{m\alpha} M^1_{\alpha n} - \overline{A}^1_{m\alpha} \overline{M}^1_{\alpha n} \right) \tag{A.6}$$

where M^1 is the inverse of L, given by

$$L^1_{j\alpha} = -n_i C^1_{ijkm} \left(m_m + p^1_{\alpha} n_m\right) A^1_{k\alpha} \tag{A.7}$$

for $\alpha, j \in \{1,2,3\}$.

To determineE^0, the Eshelby-Stroh constants for medium 2 (the twin), $(p^2_{\alpha}, A^2_{k\alpha})$, must also be determined by solving the equations

$$C^2_{ijkm} \left(m_i + p^2_{\alpha} n_i\right) \left(m_m + p^2_{\alpha} n_m\right) A^2_{k\alpha} = 0 \tag{A.8}$$

$$\| \left(C^2_{ijkm} \left(m_i + p^2_{\alpha} n_i\right) \left(m_m + p^2_{\alpha} n_m\right) \right) \| = 0 \tag{A.9}$$

where $\hat{n}$ is normal to the TB, parallel to $[\overline{111}]_{\mathrm{M}}$, and $\hat{m}$ is parallel to $[\overline{1}2\overline{1}]_{\mathrm{M}}$ along the TB, and C^2_{ijkm} are the elastic constants of the anisotropic medium 2 (the twin) in the $\hat{t} = \hat{m} \times \hat{n} - \hat{m} - \hat{n}$ coordinate system. Subsequently, we can calculate

$$\begin{aligned} L^2_{j\alpha} &= -n_i C^2_{ijkm} \left(m_m + p^2_{\alpha} n_m\right) A^2_{k\alpha} \\ M^2_{j\alpha} &= \left(L^2\right)^{-1}_{j\alpha} \end{aligned} \tag{A.10}$$

for $\alpha, j \in \{1,2,3\}$. And following the derivation in ref. (Bacon et al., 1980) the prelogarithmic factor E^{1-2} is given by

$$E^0 = \frac{-1}{2\pi i} G_{js} b_j b_s \tag{A.11}$$

where G is the inverse of the matrix F, given by

$$F_{si} = \sum_{\alpha=1}^{6} \left(A^1_{s\alpha} M^1_{\alpha i} + A^2_{s\alpha} M^2_{\alpha i} \right) \tag{A.12}$$

Thus, the pre-logarithmic factors E^0 and E^{∞} for all D-TB reactions are calculated form equations (A.11) and (A.4), listed in Table 6 for reactions I-III.

Appendix B. Determining Peierls stress of incident leading partial

The Peierls stress of the incident leading partial, τ_p^{LP}, corresponds to the lattice-friction stress which the incident leading partial must overcome as it approaches the TB. The coordinate system $\hat{m} - \hat{n} - \hat{t}$ is defined for the partial, where $\hat{n}$ is normal to the slip plane $(\hat{n} \| [\overline{1}1\overline{1}]_{\mathrm{M}})$, $\hat{m}$ is parallel to $[\overline{121}]_{\mathrm{M}}$, and $\hat{t} \| [10\overline{1}]_{\mathrm{M}}$ is parallel to the dislocation line. The leading partial is modeled as a Peierls dislocation, with its disregistry distribution and dislocation density distribution given by the equations (the reader is referred to Section 2.1.1 for a brief introduction on Peierls dislocations):

$$f(x) = b_{LP} \left(\frac{1}{2} + \frac{1}{\pi} \tan^{-1} \left(\frac{x - s}{\xi} \right) \right); \rho(x) = \frac{b_{LP} \xi}{\pi \left((x - s)^2 + \xi^2 \right)} \tag{B.1}$$

where x is the spatial coordinate along $\hat{m}$. First, the equilibrium core-width, ξ, of the leading partial needs to be determined as it

critically influences the Peierls stress. The core-width that minimizes the total energy of the dislocation is the equilibrium core-width, given by Eq. (B.2). The total energy is a sum total of the atomistic misft energy in the dislocation core and the continuum strain energy of the disregistry, given by Eq. (B.3).

$$\xi_0 = \underset{\xi}{\text{argmin}} E_{\text{TOTAL}}(\xi) \tag{B.2}$$

$$E_{\text{TOTAL}}(\xi) = E_{\text{ELASTIC}}(\xi) + E_{\text{MISFIT}}(\xi) \tag{B.3}$$

The misfit energy $E_{\text{MISFIT}}(\xi)$ depends on the Generalized Stacking Fault Energy (GSFE) landscape, $\gamma_1(u)$, for $0 \le u \le b_{LP}$, given by the equation

$$\gamma_1(u) = \begin{cases} \gamma_{\text{isf}} + \left(\frac{\gamma_{\text{us}} - \gamma_{\text{isf}}}{2}\right)\left(1 - \cos\left(\frac{2\pi u}{b_{LP}}\right)\right) & \text{for } 0 \le u \le \frac{b_{LP}}{2} \\ \frac{\gamma_{\text{us}}}{2}\left(1 - \cos\left(\frac{2\pi u}{b_{LP}}\right)\right) & \text{for } \frac{b_{LP}}{2} \le u \le b_{LP} \end{cases} \tag{B.4}$$

where γ_{isf} is the stable intrinsic stacking fault energy and γ_{us} is the unstable stacking fault energy on the GPFE curve. The incident leading partial, modeled by the Eq. (B.1), is positioned at $s = 0$ on the slip plane, and leads a stacking fault in its wake (in the region $-\infty < x < 0$), schematically represented in Fig. A2(a). The misfit energy of the dislocation's core is computed excluding the energy of the fault in its wake. Consequently, for a given core width of the incident leading partial, its misfit energy is calculated as,

$$E_{\text{MISFIT}}(\xi) = \left(\sum_{m=-\text{M}_{\max}}^{\text{M}_{\max}} \gamma_1(f(ma'))a' - \gamma_{\text{isf}}\text{M}_{\max}a' \right) \tag{B.5}$$

where a' represents the periodicity in energy barriers and is equal to the magnitude of the Burgers vector itself i.e. $a' = b_{LP}$. Note that the calculated misfit energy $E_{\text{MISFIT}}(\xi)$ is taken per unit length of the dislocation line. It can be computationally verified that $E_{\text{MISFIT}}(\xi)$ converges as $\text{M}_{\max}$is increased. A large value of $\text{M}_{\max} = 1000$ is chosen.

Next, the elastic energy of the dislocation is determined as a function of its core-width, i.e. $E_{\text{ELASTIC}}(\xi)$. The elastic energy is determined by solving for the strain-fields numerically around the core of the dislocation and then spatially integrating the strain-energy density. To determine the strain-fields corresponding to the dislocation core, we discretize the dislocation density as an aggregate of fractional dislocations with Burgers vectors $\Delta b_i = \rho(x_i)\Delta x$, where $\Delta x = 0.02 b_{LP}$ is the chosen discretization step size (refer Fig. A2). The strain-fields corresponding to each fractional will be determined and superposed at each location.

To determine the strain-fields of the fractional dislocations, the anisotropic Eshelby-Stroh (E-S) formalism is employed. Since this is a formalism within linear elasticity, the displacement-field components, u_k, and strain-field components, ε_{kl}, scale linearly with the magnitude of the Burgers vector of the dislocation. Thus, it is sufficient to determine the E-S constants once for a full dislocation with

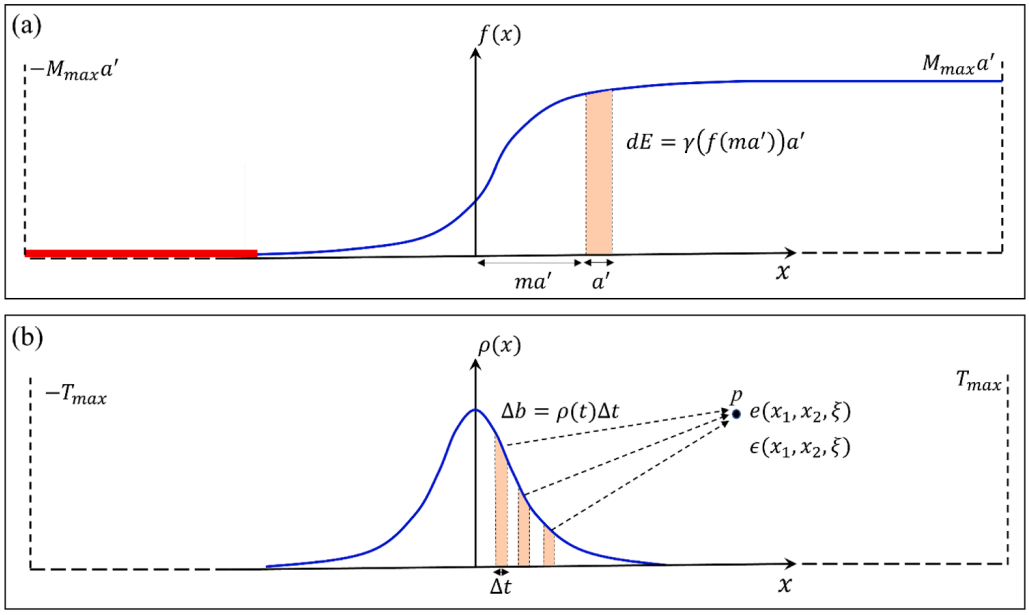

Fig. A2. (a) Calculation of misfit energy from the disregistry distribution $f(x)$ at discrete positions ma', where integer m varies between $-M_{\max}$ and $M_{\max}$ and a' is the periodicity in energy barriers as discussed in the main text (b) Calculation of strain energy from the dislocation density distribution $\rho(x)$, where the strain field $e(x_1, x_2, \xi)$ from fractional dislocations $\Delta b = \rho(t)\Delta t$ are superposed to yield the net strain at spatial location $p(x_1, x_2)$ and consequently the strain-energy density $\in (x_1, x_2, \xi)$, then integrated over space to yield the total strain-energy for the Peierls dislocation

unit Burgers vector $\widehat{b}_{LP}$, along the direction of the leading partial's Burgers vector $\overrightarrow{b}_{LP}$. Then, for each fractional dislocation $\Delta b_i = \rho(x_i)\Delta x$, the displacement-fields and consequently strain-fields are scaled as $u_l \rightarrow (\Delta b_i)u_l$ and $\varepsilon_{kl} \rightarrow (\Delta b_i)\varepsilon_{kl}$ respectively. Thus, applying the E-S formalism for a unit Burgers vector $\widehat{b}_{LP}$, the displacement-field at a position $\overrightarrow{x}$, is given by the equation:

$$u_i = \frac{1}{2\pi i}\sum_{\alpha=1}^{6}\eta_\alpha A_{i\alpha}L_{s\alpha}b_s \ln(x_1 + p_\alpha x_2) \tag{B.6}$$

where $x_1 = \widehat{m}.\overrightarrow{x}$, $x_2 = \widehat{n}.\overrightarrow{x}$, $\eta_\alpha = 1$ for $\alpha \in \{1,2,3\}$ and $\eta_\alpha = -1$ for $\alpha \in \{4,5,6\}$, and $\{p_\alpha, A_{i\alpha}, L_{s\alpha}\}$ are the E-S constants. The E-S constants are solved for from the equations:

$$\| \left(C^1_{ijkm}(m_i + p_\alpha n_i)(m_m + p_\alpha n_m) \right. \| = 0 \tag{B.7}$$

$$C^1_{ijkm}(m_i + p_\alpha n_i)(m_m + p_\alpha n_m)A_{k\alpha} = 0 \tag{B.8}$$

$$L_{j\alpha} = -n_i C_{ijkm}(m_m + p_\alpha n_m)A_{k\alpha} \tag{B.9}$$

where C_{ijkl} is the stiffness tensor associated with the matrix in the $\widehat{t} - \widehat{m} - \widehat{n}$ coordinate system. The strain-field at any point, $\overrightarrow{x} = (x_1, x_2, x_3)$, is given by

$$\varepsilon_{ij} = \frac{1}{2}\left(\frac{\partial u_i}{\partial x_j} + \frac{\partial u_j}{\partial x_i}\right) \tag{B.10}$$

Substituting equation (B.6) in (B.10), we have the strain-field given by

$$\varepsilon_{ij}(x_1, x_2) = \frac{1}{4\pi i}\sum_{\alpha=1}^{6}\frac{\eta_\alpha L_{s\alpha}b_s}{(x_1 + p_\alpha x_2)}\left(A_{i\alpha}\left(\delta_{1\mathrm{j}} + p_\alpha\delta_{2\mathrm{j}}\right) + A_{j\alpha}(\delta_{1\mathrm{i}} + p_\alpha\delta_{2\mathrm{i}})\right) \tag{B.11}$$

Recall that the strain-field given by (B.11) is for a dislocation with unit Burgers $\widehat{b}_{LP}$. To determine the strain-field of the full Peierls dislocation, the contribution from each fractional dislocation Δb_i must be numerically integrated. This is represented by the equation,

$$e_{ab}(x_1, x_2, \xi) = \int_{-\infty}^{-\infty}\varepsilon_{ab}(x_1 - t, x_2)\rho(t, \xi)\mathrm{d}t \approx \int_{-T_{\max}}^{T_{\max}}\varepsilon_{ab}(x_1 - t, x_2)\rho(t, \xi)\mathrm{d}t \tag{B.12}$$

Given the strain-field of the Peierls dislocation, the strain-energy density can be determined as

$$\in (x_1, x_2, \xi) = \frac{1}{2}C^1_{abcd}e_{ab}(x_1, x_2, \xi)e_{cd}(x_1, x_2, \xi) \tag{B.13}$$

Both the strain-field and the strain-energy density are independent of $x_3 = \widehat{t}.\overrightarrow{x}$, which is the coordinate parallel to the dislocation line. Consequently, the strain-energy is calculated per unit length of the dislocation line, given by

$$E_{\mathrm{ELASTIC}}(\xi) = \int_{-\mathrm{X}_{\max}}^{\mathrm{X}_{\max}}\int_{-\mathrm{X}_{\max}}^{\mathrm{X}_{\max}} \in (x_1, x_2, \xi)\mathrm{d}x_1\mathrm{d}x_2 = \int_{-\mathrm{X}_{\max}}^{\mathrm{X}_{\max}}\int_{-\mathrm{X}_{\max}}^{\mathrm{X}_{\max}}\int_{-T_{\max}}^{T_{\max}}\varepsilon_{ab}(x_1 - t, x_2)\rho(t, \xi)\mathrm{d}t\,\mathrm{d}x_1\mathrm{d}x_2 \tag{B.14}$$

The integrations in equation is done using standard numerical routines in MATLAB® (*integ* function) that employ adaptive quadrature. The integration limits are chosen to be sufficiently large given by $T_{\max} = 100b_{LP}$ and $X_{\max} = 100b_{LP}$.

Having calculated the continuum-elastic strain energy $E_{\mathrm{ELASTIC}}(\xi)$ (equation (B.14)) and atomistic misfit energy $E_{\mathrm{MISFIT}}(\xi)$ (equation (B.5)) of the Peierls dislocation, the total energy $E_{\mathrm{TOTAL}}(\xi)$ can now be determined as a function of its core-width ξ (equation (B.3)). Then, the total energy is minimized with respect to the dislocation core-width ξ to obtain the equilibrium value ξ_0,

$$\left.\frac{\partial E_{\mathrm{TOTAL}}(\xi)}{\partial\xi}\right|_{\xi_0} = 0 \tag{B.15}$$

The minimization is performed using standard routines in MATLAB® (*fminsearch* function). Now, that the equilibrium core-width is known, the lattice friction stress τ_p^{LP} is determined by considering the displacement of the Peierls dislocation by one Burgers vector in the lattice. Thus the disregistry distribution is changing position given by $0 \le u \le b_{LP}$. At each position, u, the misfit energy $E_{\mathrm{MISFIT}}(u)$ is computed, given by the equation,

$$E_{\mathrm{MISFIT}}(u) = \left(\sum_{m=-\mathrm{M}_{\max}}^{\mathrm{M}_{\max}}\gamma_1(f(ma' - u))a' - \gamma_{\mathrm{isf}}(\mathrm{M}_{\max}a' + u)\right) \tag{B.16}$$

where $a' = b_{LP}$, and the calculated equilibrium core-width ξ_0 is used for the disregistry distribution f. As before, it can be verified that $E_{\mathrm{MISFIT}}(\xi)$ converges as $\mathrm{M}_{\max}$is increased. A large value of $\mathrm{M}_{\max} = 1000$ is chosen. Finally, the Peierls stress τ_p^{LP} is calculated by the

maximum slope on this misfit energy landscape, given by

$$\tau_p^{LP} = \max\left\{\frac{1}{b_{LP}}\frac{dE_{\text{MISFIT}}(u)}{du}\right\} \tag{B.17}$$

This Peierls stress is used in stage 1 of the EDC model, in Section 2.1.2.

Appendix C. Calculation of anisotropic elastic parameter K

In stage 2 of the EDC model (Section 2.1.3), the elastic energy of the system E_{ELASTIC} must be determined, specifically the manner in which it varies, as a function of the state variables (s_i, ξ_i) for $i = 1,2,3,4$. As any of the state variables vary, the elastic energy changes only because of the change in the relative position of fractional dislocations from each other. In other words, consider the fractional dislocation $\mathrm{d}b_i = \rho_i(x)\mathrm{d}x$, residing within the dislocation core of the i^{th} dislocation participating in the reaction. As the core-structures evolve during the D-TB reaction (reflected by a change in (s_i, ξ_i) state variables), its strain-energy of interaction with the fractional dislocation $\mathrm{d}b_j = \rho_j(t)\mathrm{d}t$, residing in the core of the j^{th} dislocation ($j = 1,2,3,4$), varies because of a change in their relative positions, $\overrightarrow{R}(x,t) = x\hat{s}_i - t\hat{s}_j$ (where $\hat{s}_i$ is the unit vector along the direction of increasing s_i as shown in Fig. 4). In stage 2 of the model, all cores are close to the TB (i.e at distances smaller than the classical core width, i.e. $s_i < r_c = 5b_{LP}$). Consequently, from a continuum standpoint, it is sufficient to consider them to be directly on the TB between two anisotropic media. In other words, as far as the strain-energy is concerned, we only need to consider the relative distance $|\overrightarrow{R}(x,t)| = R(x,t)$ between the fractionals, modeling both to be directly on the TB. The strain-energy of interaction is then given by the expression

$$\mathrm{d}E_{\text{ELASTIC}} = \frac{K_{ij}}{2\pi}\left|\hat{b}_i.\hat{b}_j\right|\mathrm{d}b_i\mathrm{d}b_j\ln R = \frac{K_{ij}}{2\pi}\left|\hat{b}_i.\hat{b}_j\right|\rho_i(x)\rho_j(t)\ln R(x,t)\mathrm{d}x\mathrm{d}t \tag{C.1}$$

where $\hat{b}_i$ and $\hat{b}_j$ represent unit vectors along the Burgers vectors $\overrightarrow{b}_i$ and $\overrightarrow{b}_j$ respectively. The above expression has been priorly employed in anisotropic modeling of dislocation cores in BCC materials (Alkan and Sehitoglu, 2019; Kroupa and Lejček, 1972; Lejček and Kroupa, 1981). The challenge however is in the determination of the right value of K_{ij} capturing the anisotropy in the interaction. Several approaches have been proposed in this regard (Foreman, 1955), but none are faithful from a strain-energy standpoint and thus not appropriate for the model. In this study, we back-calculate K_{ij} from an analytically derived strain-energy calculation from the anisotropic Eshelby-Stroh formalism. This is discussed below. Having determined the right values of K_{ij}, the cumulative interaction of all such fractional pairs within all cores of participating dislocations yields the E_{ELASTIC} energy of the system at the given state (s_i, ξ_i). This is given by:

$$E_{\text{ELASTIC}} = \sum_{i=1}^{4}\sum_{j=i}^{4}\frac{K_{ij}}{2\pi}\int_0^{s_i^{\max}}\int_0^{s_j^{\max}}\rho_i(x)\rho_j(t)\ln R(x,t)\mathrm{d}x\mathrm{d}t \tag{C.2}$$

Now, we consider the calculation of the anisotropic parameter K_{ij} that captures the anisotropy in the strain-interaction energy between Burgers vectors $\overrightarrow{b}_i$ and $\overrightarrow{b}_j$ in the reaction. To determine K_{ij} it is sufficient to consider unit vectors along the Burgers vector

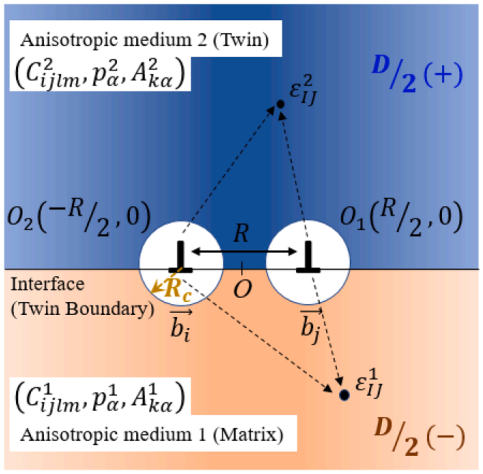

Fig. A3. Computing elastic strain-energy of a two-dislocation system positioned on an interface separating two anisotropic media; the Burgers vectors of the two dislocations are given by $\overrightarrow{b}_i$ and $\overrightarrow{b}_j$ respectively positioned at $O_1(R/2, 0)$ and $O_2(-R/2, 0)$ respectively; the anisotropic media are characterized by their respective elastic constants $C^{1,2}_{IJKL}$ and anisotropic Eshelby-Stroh constants $p^{1,2}_\alpha$, $A^{1,2}_{K\alpha}$; the strain-fields of both dislocations are superposed to determine the total strain-field ε^1_{IJ} in domain 1 and ε^2_{IJ} in domain 2, consequently integrating the strain-energy density over the rectangular domain, only excluding the cores of both dislocations demarcated by a circular region of radius R_c

directions given by $\widehat{b}_i$ and $\widehat{b}_j$, as the magnitude of the Burgers vector does not affect its value. The unit dislocations are presumed to be separated by distance R along the TB (Fig. A3). We analytically derive the strain-fields using the anisotropic Eshelby-Stroh (E-S) formalism as applied to anisotropic interfaces, where in this case the interface is the TB. Having solved for the strain-field surrounding the two-dislocation system, the strain-energy density distribution is determined and numerically integrated to yield the total strain-energy of the system. Subsequently, the value of K_{ij} is back-calculated as one that captures the change in strain-energy as a function of varying R. This procedure is elaborated further below.

First, the anisotropic E-S constants corresponding to Burgers vectors $\overrightarrow{b}_i$ and $\overrightarrow{b}_j$ are solved for. The coordinate system $\widehat{m}\ -\widehat{n}\ -\widehat{t}$ is defined (consistent with Fig. 2), where $\widehat{n}$ is normal to the TB ($\widehat{n}\|[\overline{1}11]_{\mathrm{M}}$), $\widehat{m}$ is parallel to $[1\overline{2}1]_{\mathrm{M}}$, and $\widehat{t}\|[10\overline{1}]_{\mathrm{M}}$ is parallel to the dislocation lines. In this orientation, the dislocations are positioned as follows: $\overrightarrow{b}_i$ at $(R/2, 0, 0)$ and $\overrightarrow{b}_j$ at $(-R/2, 0, 0)$. Let the anisotropic elastic constants of medium 1 (the matrix) and medium 2 (the twin), in the above orientation be given by C^1_{ABCD} and C^2_{ABCD} respectively.

The anisotropic E-S constants to be determined for the strain-field of dislocation $\overrightarrow{b}_i$ are given by $(p^1_\alpha, A^1_{K\alpha}, E^{1i}_\alpha)$ in medium 1 and $(p^2_\alpha, A^2_{K\alpha}, E^{2i}_\alpha)$ in medium 2, where the upper-case alphabetical indices vary as $K = 1,2,3$, the lower-case index varies as $i = 1, 2, 3, 4$ and, the Greek index varies as $\alpha = 1, 2, 3, 4, 5, 6$. Similarly for dislocation $\overrightarrow{b}_j$, the constants are $(p^1_\alpha, A^1_{K\alpha}, E^{1j}_\alpha)$ in medium 1 and $(p^2_\alpha, A^2_{K\alpha}, E^{2j}_\alpha)$ in medium 2. The equations from the formalism are listed below. The reader is referred to (Barnett and Lothe, 1974; Ting, 1996) for a more detailed exposition. The constants p^1_α and p^2_α are solved for from the equations:

$$\| C^1_{IJKL}\left(m_I + p^1_\alpha n_I\right)\left(m_L + p^1_\alpha n_L\right) \| = 0 \tag{C.3}$$

$$\| C^2_{IJKL}\left(m_I + p^2_\alpha n_I\right)\left(m_L + p^2_\alpha n_L\right) \| = 0 \tag{C.4}$$

The complex constants are ordered such that for $\alpha = 1, 2, 3$, the imaginary part of p^1_α, p^2_α, is positive, and $p^1_{\alpha+3} = \overline{p}^1_\alpha, p^2_{\alpha+3} = \overline{p}^2_\alpha$, where the bar represents the complex-conjugate. The constants $A^{1,2}_{K\alpha}$ are solved for from the equations:

$$C^1_{IJKL}\left(m_I + p^1_\alpha n_I\right)\left(m_L + p^1_\alpha n_L\right)A^1_{K\alpha} = 0 \tag{C.5}$$

$$C^2_{IJKL}\left(m_I + p^2_\alpha n_I\right)\left(m_L + p^2_\alpha n_L\right)A^2_{K\alpha} = 0 \tag{C.6}$$

From $(p^1_\alpha, A^1_{K\alpha})$, $(p^2_\alpha, A^2_{K\alpha})$, the constants $L^1_{I\alpha}$, $L^2_{I\alpha}$, are derived as:

$$L^1_{I\alpha} = -n_J C^1_{IJKL}\left(m_L + p^1_\alpha n_L\right)A^1_{K\alpha} \tag{C.7}$$

$$L^2_{I\alpha} = -n_J C^2_{IJKL}\left(m_L + p^2_\alpha n_L\right)A^2_{K\alpha} \tag{C.8}$$

Finally, the constants E^{i1}_α and E^{i2}_α are solved for from the equations,

$$\sum_{\alpha=1}^{6}\left(A^2_{I\alpha}E^{2i}_\alpha - A^1_{I\alpha}E^{1i}_\alpha\right) = 0 \tag{C.9}$$

$$\sum_{\alpha=1}^{6}\left(\eta_\alpha A^2_{I\alpha}E^{2i}_\alpha + \eta_\alpha A^1_{I\alpha}E^{1i}_\alpha\right) = 2\left(\overrightarrow{b}_i\right)_I \tag{C.10}$$

$$\sum_{\alpha=1}^{6}\left(L^2_{I\alpha}E^{2i}_\alpha - L^1_{I\alpha}E^{1i}_\alpha\right) = 0 \tag{C.11}$$

$$\sum_{\alpha=1}^{6}\left(\eta_\alpha L^2_{I\alpha}E^{2i}_\alpha + \eta_\alpha L^1_{I\alpha}E^{1i}_\alpha\right) = 0 \tag{C.12}$$

where $\eta_\alpha = 1$ for $\alpha \in \{1, 2, 3\}$ and $\eta_\alpha = -1$ for $\alpha \in \{4, 5, 6\}$ and $(\overrightarrow{b}_i)_I$ represents the I^{th} component of the dislocation $\overrightarrow{b}_i$. While the constants $(p^1_\alpha, A^1_{K\alpha})$, $(p^2_\alpha, A^2_{K\alpha})$, remain same for the dislocation $\overrightarrow{b}_j$, the constants E^{1j}_α and E^{2j}_α are solved for from the equations:

$$\sum_{\alpha=1}^{6}\left(A^2_{I\alpha}E^{2j}_\alpha - A^1_{I\alpha}E^{1j}_\alpha\right) = 0 \tag{C.13}$$

$$\sum_{\alpha=1}^{6}\left(\eta_\alpha A^2_{I\alpha}E^{2j}_\alpha + \eta_\alpha A^1_{I\alpha}E^{1j}_\alpha\right) = 2\left(\overrightarrow{b}_j\right)_I \tag{C.14}$$

$$\sum_{\alpha=1}^{6}\left(L_{I\alpha}^{2}E_{\alpha}^{2j}-L_{I\alpha}^{1}E_{\alpha}^{1j}\right)=0 \tag{C.15}$$

$$\sum_{\alpha=1}^{6}\left(\eta_{\alpha}L_{I\alpha}^{2}E_{\alpha}^{2j}+\eta_{\alpha}L_{I\alpha}^{1}E_{\alpha}^{1j}\right)=0 \tag{C.16}$$

Given the anisotropic E-S constants, the vector displacement-fields u_I^{1i} (I^{th} component, from dislocation $\vec{b}_i$, in medium 1), u_I^{2i} (I^{th} component, from dislocation $\vec{b}_i$, in medium 2), u_I^{1j} (I^{th} component, from dislocation $\vec{b}_j$, in medium 1) and u_I^{2j} (I^{th} component, from dislocation $\vec{b}_j$, in medium 2) can be computed from the equations:

$$u_I^{1i}(x_1,x_2)=\frac{1}{2\pi\sqrt{-1}}\sum_{\alpha=1}^{6}A_{I\alpha}^{1}E_{\alpha}^{1i}\ln\left(x_1-R/2+p_{\alpha}^{1}x_2\right) \tag{C.17}$$

$$u_I^{2i}(x_1,x_2)=\frac{1}{2\pi\sqrt{-1}}\sum_{\alpha=1}^{6}A_{I\alpha}^{2}E_{\alpha}^{2i}\ln\left(x_1-R/2+p_{\alpha}^{2}x_2\right) \tag{C.18}$$

$$u_I^{1j}(x_1,x_2)=\frac{1}{2\pi\sqrt{-1}}\sum_{\alpha=1}^{6}A_{I\alpha}^{1}E_{\alpha}^{1j}\ln\left(x_1+R/2+p_{\alpha}^{1}x_2\right) \tag{C.19}$$

$$u_I^{2j}(x_1,x_2)=\frac{1}{2\pi\sqrt{-1}}\sum_{\alpha=1}^{6}A_{I\alpha}^{2}E_{\alpha}^{2j}\ln\left(x_1+R/2+p_{\alpha}^{2}x_2\right) \tag{C.20}$$

where $x_1=\hat{m}.\vec{x}$ and $x_2=\hat{n}.\vec{x}$. The displacement and strain-fields are independent of $x_3=\hat{t}.\vec{x}$, since $\hat{t}$ is along the dislocation line. From the displacement-fields, the strain-field ε_{IJ}^{1i} (IJ^{th} component of the strain-tensor in medium 1, caused by dislocation $\vec{b}_i$) can be computed by taking the symmetric displacement gradient as follows:

$$\varepsilon_{IJ}^{1i}(x_1,x_2)=\frac{1}{2}\left(\frac{\partial u_I^{1i}}{\partial x_J}+\frac{\partial u_J^{1i}}{\partial x_I}\right) \tag{C.21}$$

The remaining strain-fields ε_{IJ}^{2i}, ε_{IJ}^{1j}, and ε_{IJ}^{2j}, can also be computed following equation (C.21). The net striain-field in medium 1, caused by both dislocations is then given by:

$$\varepsilon_{IJ}^{1}(x_1,x_2)=\varepsilon_{IJ}^{1i}(x_1,x_2)+\varepsilon_{IJ}^{1j}(x_1,x_2) \tag{C.22}$$

The strain-field in medium 2 can be determined similarly. The total strain-energy of the two-dislocation system can then be computed as

$$E_{ij}(R)=\int_{D2(+)}\int C_{IJKL}^{2}\varepsilon_{IJ}^{2}\varepsilon_{KL}^{2}\mathrm{d}x_1\mathrm{d}x_2+\int_{D2(-)}\int C_{IJKL}^{1}\varepsilon_{IJ}^{1}\varepsilon_{KL}^{1}\mathrm{d}x_1\mathrm{d}x_2 \tag{C.23}$$

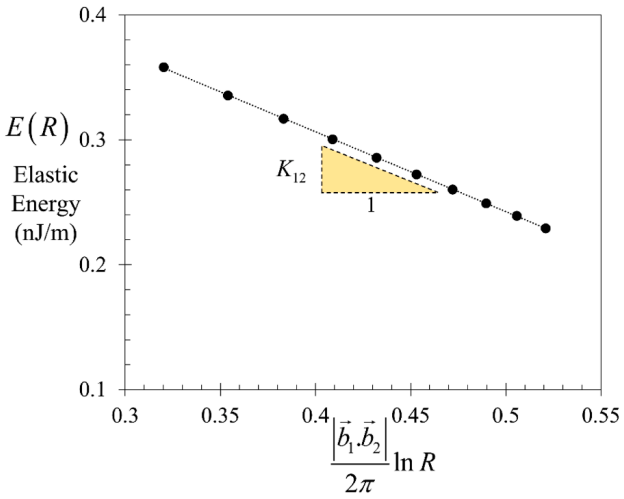

Fig. A4. Determining anisotropic interaction parameter K_{ij} from the variation of strain-energy $E(R)$with distance between dislocations $\vec{b}_i$ and $\vec{b}_j$, given by R; in this plot $i=1$ and $j=2$, and from Table 1, $\vec{b}_1=a/6[21\bar{1}]_{\text{M}}$ and $\vec{b}_2=a/6[2\bar{1}1]_{\text{M}}$

where the domain D is a rectangular region of dimensions $150b_{LP} \times 150b_{LP}$ centered at O, and excluding the circular cores around individual dislocations, respectively centered at $O_1(R/2, 0)$ and $O_2(-R/2, 0)$ with radius $R_c = 5b_{LP}$ (refer Fig. A3). And the domains $D/2(+)$ and $D/2(-)$, in equation (C.23) represent two halves of the domain D in medium 2 and medium 1 respectively (refer Fig. A3). The integrals in equation (C.23) are computed numerically on a discretized grid over the domain.

The anisotropic parameter K_{ij} is determined by considering the variation of $E_{ij}(R)$ as a function of R. As can be seen from Fig. 11, $E_{ij}(R)$ varies linearly with $\ln R$, and its behavior is well-modeled by the equation:

$$E_{ij}(R) = C_0 + \frac{K_{ij}}{2\pi}\left|\vec{b}\,.\,\vec{b}_j\right|\ln R \tag{C.24}$$

Consequently, K_{ij} is determined as the slope of the linear fit. It is worth emphasizing that $E_{ij}(R)$ was derived analytically from a fully-anisotropic elastic approach and its behavior with varying R (Fig. A4) is used to back-calculate the anisotropic interaction parameter K_{ij}. This parameter, determined for all dislocations in the reaction, ultimately affords a convenient and accurate evaluation of E_{ELASTIC} as employed in equations (C.2) and (2.16). Calculated interaction parameters for Nickel (Ni) in slip-incorporation reaction I, II and III are listed in Tables 3, 4 and 5 respectively. The respective parameters for high-entropy alloy FeNiCoCrMn for slip-incorporation reaction V are listed in Table 10.

Appendix D. Generalized Stacking Fault Energies of Ni-based alloys from Molecular Statics (MS)

The calculation of the Generalized Stacking Fault Energy (GSFE) curves for the Ni-Ti and Ni-Co alloys considered in this study are detailed here. These curves are determined within a Molecular Statics (MS) simulation framework carried out in LAMMPS (Plimpton, 1995), and resulting atomic structures are visualized in OVITO (Stukowski, 2009). The procedure is elaborated using the Ni-Ti solid-solution as the example and the same procedure is applied for the Ni-Co system. The interatomic potential developed in (Ren and Sehitoglu, 2016) is employed for the Ni-Ti system and for the Ni-Co system, the potential developed in (Béland et al., 2016) is employed. First, the equilibrium atomic structures of the solid solution must be constructed within the simulation framework.

The simulation cell was created such that x-y-z directions are along $[121] - [\bar{1}11] - [1\bar{1}0]$ crystallographic directions. The cell is populated with a Face-Centered-Cubic crystal structure with Ni atoms and randomly-substituted solute atoms, Ti in this case. The number of substituted atoms is controlled based on the required final composition (i.e. 10%Ti or 20%Ti etc.). Periodic boundary conditions are enforced across all boundaries of the simulation box. Since the alloying was done randomly, there can be unphysical effects such as local clusters of solutes or other unphysical distributions introduced by the artificial construction of the alloy structure. To homogenize the alloying, a Monte-Carlo simulation is performed where solute atoms (Ti) exchange/swap positions with matrix atoms (Ni) (*atom swap* function in LAMMPS) over several steps until the energy of the atomic structure converges to an energy-minimized state (Sadigh et al., 2012). This minimization and associated structure transitions are highlighted in Fig. A5. At the energy-minimized state, the alloy structure is said to be homogenized with an even distribution of the solute atoms in the matrix, and thus of higher physical fidelity than the starting structure. The GSFE for the alloy state is calculated for this structure.

Calculation of GSFEs for Face-Centered-Cubic (FCC) materials for the $\{111\}\langle 112\rangle$ slip system has been discussed in detail by several authors and the reader is directed to (Vítek, 1968) for a detailed exposition on the topic. Briefly, the GSFE is calculated by starting from an equilibrium atomic structure of the alloy and then introducing a rigid disregistry on the $\{111\}$ slip-plane in the direction of the Burgers vector i.e. $\vec{b} = a/6\langle 112\rangle$. This disregistry is introduced by rigidly displacing one half of the equilibrium structure with respect to the other half, by displacement u along the direction of the Burgers vector $\vec{b}$ on the slip plane. The boundary conditions of the simulation along the lateral directions on the slip plane are specified to be periodic to simulate the bulk material. And the boundary conditions normal to the slip plane (top and bottom boundaries) are specified to be shrink-wrapped. A frozen-layer of atoms with layer

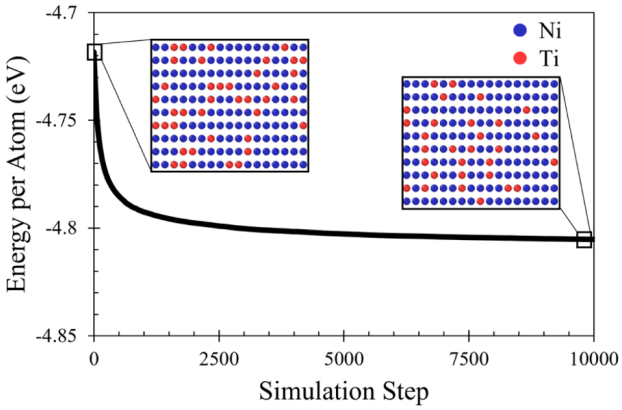

Fig. A5. Equilibration of Ni-20%Ti alloy atomic structure during Monte-Carlo simulation; the inset shows snapshots of the atomic structure at different simulation steps, indicating the homogenization of the solute distribution in the matrix with progress of the simulation, converging to an energy-minimized state

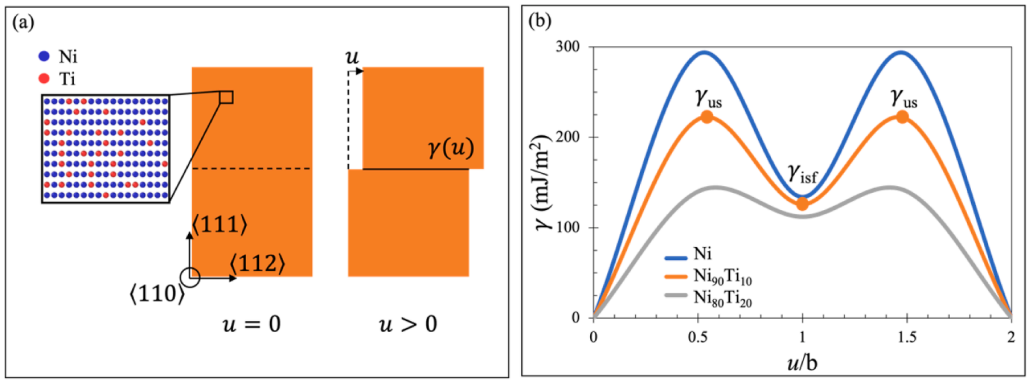

Fig. A6. (a) The procedure to calculate the GSFE is schematically indicated, determined from the fault energies γ(u) at varying positions of disregistry u introduced on the $\{111\}\langle 112\rangle$ slip system of the FCC structure (a) Generalized Stacking Fault Energy (GSFE) curves for the Ni-Ti system determined using Molecular Statics (MS) simulations from the interatomic potential developed in (Ren and Sehitoglu, 2016)

thickness higher than the potential's cutoff distance is specified at the top and bottom boundaries, where all atomic motions are arrested. This frozen layer represents the bulk material away from the plane of disregistry that is unaffected by the introduced disregistry. The atoms within the simulation box not in the frozen layer will henceforth be referred to as the "mobile" region. With this setup, at each position of disregistry u, a MS equilibration is carried out where the energy of the structure is minimized allowing the atomic positions in the mobile region to relax in all directions except in the direction of displacement (i.e. along $\overrightarrow{b}$). The minimized energy at each u yields the stacking fault energy $\gamma(u)$ at that position of disregistry. In this manner, the entire GSFE curve can be constructed. For FCC materials, there are only two critical points, i.e. two critical values of u, where the stacking fault energy $\gamma(u)$ needs to be determined. The GSFE can be well-interpolated using trigonometric functions between these points. These two points are the unstable stacking fault energy γ_{us} obtained at $u = b/2$ and the stable intrinsic stacking fault energy γ_{isf} at $u = b$. These two energies are obtained for all the Ni-based alloys considered in this study (listed in Table 6), and indicated on the respective GSFE curves in Fig. A6. As can be seen, there is a considerable decrease in the fault energies with increasing Ti content. Additionally, the difference between γ_{us} and γ_{isf} is lowered with the addition of Ti which has an effect of increasing the twinnability of the material. Combining these fault energies with the EDC model ultimately affords the power to model D-TB reactions in materials for which empirical interatomic potentials do not exist.

References

Abuzaid, W.Z., Sangid, M.D., Carroll, J.D., Sehitoglu, H., Lambros, J., 2012. Slip transfer and plastic strain accumulation across grain boundaries in Hastelloy X. Journal of the Mechanics and Physics of Solids 60, 1201–1220.

Alkan, S., Chowdhury, P., Sehitoglu, H., Rateick, R.G., Maier, H.J., 2016. Role of nanotwins on fatigue crack growth resistance – Experiments and theory. International Journal of Fatigue 84, 28–39.

Alkan, S., Ojha, A., Sehitoglu, H., 2018a. The complexity of non-Schmid behavior in the CuZnAl shape memory alloy. Journal of the Mechanics and Physics of Solids 114, 238–257.

Alkan, S., Ojha, A., Sehitoglu, H., 2018b. Determination of latent hardening response for FeNiCoCrMn for twin-twin interactions. Acta Materialia 147, 149–164.

Alkan, S., Sehitoglu, H., 2017. Nonuniqueness of the fatigue threshold. International Journal of Fatigue 104, 309–321.

Alkan, S., Sehitoglu, H., 2019. Plastic flow resistance of NiTiCu shape memory alloy-theory and experiments. Acta Materialia 163, 173–188.

Alkan, S., Wu, Y., Sehitoglu, H., 2017. Giant non-Schmid effect in NiTi. Extreme Mechanics Letters 15, 38–43.

Argon, A.S., 2007. Kinematics and Kinetics in Crystal Plasticity, Strengthening Mechanisms in Crystal Plasticity. Oxford University Press, Oxford.

Bacon, D.J., Barnett, D.M., Scattergood, R.O., 1980. Anisotropic continuum theory of lattice defects. Progress in Materials Science 23, 51–262.

Bacon, D.J., Vitek, V., 2002. Atomic-scale modeling of dislocations and related properties in the hexagonal-close-packed metals. Metallurgical and Materials Transactions A 33, 721–733.

Barnett, D.M., Lothe, J., 1974. An image force theorem for dislocations in anisotropic bicrystals. Journal of Physics F: Metal Physics 4, 1618–1635.

Béland, L.K., Lu, C., Osetskiy, Y.N., Samolyuk, G.D., Caro, A., Wang, L., Stoller, R.E., 2016. Features of primary damage by high energy displacement cascades in concentrated Ni-based alloys. Journal of Applied Physics 119, 85901-85901.

Beyerlein, I.J., Tomé, C.N., 2008. A dislocation-based constitutive law for pure Zr including temperature effects. International Journal of Plasticity 24, 867–895.

Bönisch, M., Wu, Y., Sehitoglu, H., 2018. Hardening by slip-twin and twin-twin interactions in FeMnNiCoCr. Acta Materialia 153, 391–403.

Bonneville, J., Escaig, B., 1979. Cross-slipping process and the stress-orientation dependence in pure copper. Acta Metallurgica 27, 1477–1486.

Bouaziz, O., Guelton, N., 2001. Modelling of TWIP effect on work-hardening. Materials Science and Engineering: A 319-321, 246–249.

Brenne, F., Mohammed, A.S.K., Sehitoglu, H., 2020. High resolution atomic scale characterization of dislocations in high entropy alloys: Critical assessment of template matching and geometric phase analysis. Ultramicroscopy 219, 113134.

Carlton, C.E., Ferreira, P.J., 2007. What is behind the inverse Hall–Petch effect in nanocrystalline materials? Acta Materialia 55, 3749–3756.

Chassagne, M., Legros, M., Rodney, D., 2011. Atomic-scale simulation of screw dislocation/coherent twin boundary interaction in Al, Au, Cu and Ni. Acta Materialia 59, 1456–1463.

Chen, P., Wang, F., Li, B., 2019. Dislocation absorption and transmutation at $\{101\bar{2}\}$ twin boundaries in deformation of magnesium. Acta Materialia 164, 440–453.

Chen, Z., Jin, Z., Gao, H., 2007. Repulsive force between screw dislocation and coherent twin boundary in aluminum and copper. Physical Review B 75, 212104.

Chou, Y.T., 1966. On Dislocation-Boundary Interaction in an Anisotropic Aggregate. physica status solidi (b) 15, 123–127.

Chowdhury, P., Sehitoglu, H., Maier, H.J., Rateick, R., 2016. Strength prediction in NiCo alloys – The role of composition and nanotwins. International Journal of Plasticity 79, 237–258.

Chowdhury, P.B., Sehitoglu, H., Rateick, R.G., 2014. Predicting fatigue resistance of nano-twinned materials: Part I – Role of cyclic slip irreversibility and Peierls stress. International Journal of Fatigue 68, 277–291.
Chowdhury, P.B., Sehitoglu, H., Rateick, R.G., Maier, H.J., 2013. Modeling fatigue crack growth resistance of nanocrystalline alloys. Acta Materialia 61, 2531–2547.
Dang, K., Graham, J., Tomé, C.N., Capolungo, L., 2021. Three-Dimensional Interaction of $$ \left\{{10\bar{1}2} \right\} $$Twin with Tilt Boundaries in Mg: Twin and Dislocation Transmission. In: Miller, V.M., Maier, P., Jordon, J.B., Neelameggham, N.R. (Eds.), Magnesium Technology 2021. Springer International Publishing, Cham, pp. 49–51.
Duesbery, M.S., Vitek, V., 1998. Plastic anisotropy in b.c.c. transition metals. Acta Materialia 46, 1481–1492.
Eshelby, J.D., Read, W.T., Shockley, W., 1953. Anisotropic elasticity with applications to dislocation theory. Acta Metallurgica 1, 251–259.
Ezaz, T., Sangid, M.D., Sehitoglu, H., 2011. Energy barriers associated with slip–twin interactions. Philosophical Magazine 91, 1464–1488.
Fan, H., Wang, Q., El-Awady, J.A., Raabe, D., Zaiser, M., 2021. Strain rate dependency of dislocation plasticity. Nature Communications 12, 1845.
Foreman, A.J., Jaswon, M.A., Wood, J.K., 1951. Factors Controlling Dislocation Widths. Proceedings of the Physical Society. Section A 64, 156–163.
Foreman, A.J.E., 1955. Dislocation energies in anisotropic crystals. Acta Metallurgica 3, 322–330.
Gemperlová, J., 1968. Force on Dislocations in Anisotropic Bicrystals and Half-Spaces. physica status solidi (b) 30, 261–274.
Gene, S., Herbert, W., 1971. Single crystal elastic constants and calculated aggregate properties. MIT, Cambridge, MA.
Gengor, G., Mohammed, A.S.K., Sehitoglu, H., 2021. {101¯2} Twin interface structure and energetics in HCP materials. Acta Materialia, 117256.
Gong, M., Liu, G., Wang, J., Capolungo, L., Tomé, C.N., 2018. Atomistic simulations of interaction between basal <a>dislocations and three-dimensional twins in magnesium. Acta Materialia 155, 187–198.
Gu, P., Dao, M., Suresh, S., 2014a. Analysis of size-dependent slip transfer and inter-twin flow stress in a nanotwinned fcc metal. Acta Materialia 67, 409–417.
Gu, P., Dao, M., Zhu, Y., 2014b. Strengthening at nanoscaled coherent twin boundary in f.c.c. metals. Philosophical Magazine 94, 1249–1262.
Hartley, C.S., Blachon, D.L.A., 1978. Reactions of slip dislocations at coherent twin boundaries in face-centered-cubic metals. Journal of Applied Physics 49, 4788–4796.
Hirth, J.P., Lothe, J., 1983. Theory of Dislocations (2nd ed.). Journal of Applied Mechanics 50, 476–477.
Imrich, P.J., Kirchlechner, C., Motz, C., Dehm, G., 2014. Differences in deformation behavior of bicrystalline Cu micropillars containing a twin boundary or a large-angle grain boundary. Acta Materialia 73, 240–250.
Jin, J., Shevlin, S.A., Guo, Z.X., 2008. Multiscale simulation of onset plasticity during nanoindentation of Al (001) surface. Acta Materialia 56, 4358–4368.
Jin, Z.H., Gumbsch, P., Ma, E., Albe, K., Lu, K., Hahn, H., Gleiter, H., 2006. The interaction mechanism of screw dislocations with coherent twin boundaries in different face-centred cubic metals. Scripta Materialia 54, 1163–1168.
Kacher, J., Eftink, B.P., Cui, B., Robertson, I.M., 2014. Dislocation interactions with grain boundaries. Current Opinion in Solid State and. Materials Science 18, 227–243.
Kaschner, G.C., Tomé, C.N., McCabe, R.J., Misra, A., Vogel, S.C., Brown, D.W., 2007. Exploring the dislocation/twin interactions in zirconium. Materials Science and Engineering: A 463, 122–127.
Kibey, S., Liu, J.B., Johnson, D.D., Sehitoglu, H., 2007. Predicting twinning stress in fcc metals: Linking twin-energy pathways to twin nucleation. Acta Materialia 55, 6843–6851.
Kocks, U.F., Ashby, M.F., Argon, A.S., 1975. Thermodynamics and kinetics of slip, 1st ed. Pergamon Press, Oxford.
Kroupa, F., Lejček, L., 1972. Splitting of dislocations in the Peierls-Nabarro model. Czechoslovak Journal of Physics B 22, 813–825.
Kroupa, F., Vítek, V., 1967. SLIP AND THE CONCEPTION OF SPLITTING OF DISLOCATIONS IN b.c.c. METALS. Canadian Journal of Physics 45, 945–971.
Lee, J.H., Holland, T.B., Mukherjee, A.K., Zhang, X., Wang, H., 2013. Direct observation of Lomer-Cottrell Locks during strain hardening in nanocrystalline nickel by in situ TEM. Scientific Reports 3, 1061.
Lee, T.C., Robertson, I.M., Birnbaum, H.K., 1989. Prediction of slip transfer mechanisms across grain boundaries. Scripta Metallurgica 23, 799–803.
Lee, T.C., Robertson, I.M., Birnbaum, H.K., 1990. TEM in situ deformation study of the interaction of lattice dislocations with grain boundaries in metals. Philosophical Magazine A 62, 131–153.
Lejček, L., Kroupa, F., 1976. Peierls-Nabarro model of non-planar screw dislocation cores. Czechoslovak Journal of Physics B 26, 528–537.
Lejček, L., Kroupa, F., 1981. The effect of shear stress on the screw dislocation core in bcc metals. Czechoslovak Journal of Physics B 31, 719–723.
Li, N., Wang, J., Misra, A., Zhang, X., Huang, J.Y., Hirth, J.P., 2011. Twinning dislocation multiplication at a coherent twin boundary. Acta Materialia 59, 5989–5996.
Li, Z., Wang, J., Liu, W., 2018. Basal ⟨a⟩ dislocation-{1¯011} contraction twin interactions in magnesium. Computational Materials Science 155, 11–16.
Mahajan, S., 1971. Twin-slip and twin-twin interactions in Mo-35 at. % Re alloy. The Philosophical Magazine: A. Journal of Theoretical Experimental and Applied Physics 23, 781–794.
Mahajan, S., Chin, G.Y., 1973. Twin-slip, twin-twin and slip-twin interactions in Co-8 wt.% Fe alloy single crystals. Acta Metallurgica 21, 173–179.
Mohammed, A.S.K., Sehitoglu, H., 2020. Modeling the interface structure of type II twin boundary in B19′ NiTi from an atomistic and topological standpoint. Acta Materialia 183, 93–109.
Mohammed, A.S.K., Sehitoglu, H., 2021. Strain-sensitive topological evolution of twin interfaces. Acta Materialia 208, 116716.
Müllner, P., Solenthaler, C., 1997. On the effect of deformation twinning on defect densities. Materials Science and Engineering: A 230, 107–115.
Neighbours, J.R., Smith, C.S., 1954. The elastic constants of copper alloys. Acta Metallurgica 2, 591–596.
Pacheco, E.S., Mura, T., 1969. Interaction between a screw dislocation and a bimetallic interface. Journal of the Mechanics and Physics of Solids 17, 163–170.
Peierls, R., 1940. The size of a dislocation. Proceedings of the Physical Society 52, 34–37.
Plimpton, S., 1995. Fast Parallel Algorithms for Short-Range Molecular Dynamics. Journal of Computational Physics 117, 1–19.
Proust, G., Tomé, C.N., Jain, A., Agnew, S.R., 2009. Modeling the effect of twinning and detwinning during strain-path changes of magnesium alloy AZ31. International Journal of Plasticity 25, 861–880.
Püschl, W., 2002. Models for dislocation cross-slip in close-packed crystal structures: a critical review. Progress in Materials Science 47, 415–461.
Püschl, W., Schoeck, G., 1993. Calculation of cross-slip parameters in f.c.c. crystals. Materials Science and Engineering: A 164, 286–289.
Ramírez, B.R., Ghoniem, N., Po, G., 2012. Ab initio continuum model for the influence of local stress on cross-slip of screw dislocations in fcc metals. Physical Review B 86, 094115.
Rémy, L., 1977. Twin-slip interaction in f.c.c. crystals. Acta Metallurgica 25, 711–714.
Rémy, L., 1981. The interaction between slip and twinning systems and the influence of twinning on the mechanical behavior of fcc metals and alloys. Metallurgical Transactions A 12, 387–408.
Ren, G., Sehitoglu, H., 2016. Interatomic potential for the NiTi alloy and its application. Computational Materials Science 123, 19–25.
Robertson, I.M., Beaudoin, A., Al-Fadhalah, K., Chun-Ming, L., Robach, J., Wirth, B.D., Arsenlis, A., Ahn, D., Sofronis, P., 2005. Dislocation–obstacle interactions: Dynamic experiments to continuum modeling. Materials Science and Engineering: A 400-401, 245–250.
Sadigh, B., Erhart, P., Stukowski, A., Caro, A., Martinez, E., Zepeda-Ruiz, L., 2012. Scalable parallel Monte Carlo algorithm for atomistic simulations of precipitation in alloys. Physical Review B 85, 184203-184203.
Samaee, V., Dupraz, M., Pardoen, T., Van Swygenhoven, H., Schryvers, D., Idrissi, H., 2021. Deciphering the interactions between single arm dislocation sources and coherent twin boundary in nickel bi-crystal. Nature Communications 12, 962.
Sangid, M.D., Ezaz, T., Sehitoglu, H., 2012. Energetics of residual dislocations associated with slip–twin and slip–GBs interactions. Materials Science and Engineering: A 542, 21–30.
Sangid, M.D., Ezaz, T., Sehitoglu, H., Robertson, I.M., 2011. Energy of slip transmission and nucleation at grain boundaries. Acta Materialia 59, 283–296.
Schoeck, G., 1994. The generalized Peierls–Nabarro model. Philosophical Magazine A 69, 1085–1095.
Schoeck, G., 2001. The core structure, recombination energy and Peierls energy for dislocations in Al. Philosophical Magazine A 81, 1161–1176.
Schoeck, G., 2002. The core structure of dislocations in Al: a critical assessment. Materials Science and Engineering: A 333, 390–396.
Schoeck, G., 2009. The cross-slip energy unresolved. Philosophical Magazine Letters 89, 505–515.

Serra, A., Bacon, D.J., 1996. A new model for {1012} twin growth in hcp metals. Philosophical Magazine A 73, 333–343.
Serra, A., Bacon, D.J., Pond, R.C., 2002. Twins as barriers to basal slip in hexagonal-close-packed metals. Metallurgical and Materials Transactions A 33, 809–812.
Serra, A., Pond, R.C., Bacon, D.J., 1991. Computer simulation of the structure and mobility of twinning disclocations in H.C.P. Metals. Acta Metallurgica et Materialia 39, 1469–1480.
Shabib, I., Miller, R.E., 2009. Deformation characteristics and stress–strain response of nanotwinned copper via molecular dynamics simulation. Acta Materialia 57, 4364–4373.
Sidharth, R., Abuzaid, W., Sehitoglu, H., 2020a. Nano-twinning enhanced room temperature fatigue crack growth in single crystalline CoCrFeMnNi high entropy alloy. Intermetallics 126, 106919-106919.
Sidharth, R., Mohammed, A.S.K., Abuzaid, W., Sehitoglu, H., 2021. Unraveling Frequency Effects in Shape Memory Alloys: NiTi and FeMnAlNi. Shape Memory and Superelasticity.
Sidharth, R., Wu, Y., Brenne, F., Abuzaid, W., Sehitoglu, H., 2020b. Relationship Between Functional Fatigue and Structural Fatigue of Iron-Based Shape Memory Alloy FeMnNiAl. Shape Memory and Superelasticity 6, 256–272.
Sim, G.-D., Krogstad, J.A., Reddy, K.M., Xie, K.Y., Valentino, G.M., Weihs, T.P., Hemker, K.J., 2017. Nanotwinned metal MEMS films with unprecedented strength and stability. Science Advances 3 e1700685-e1700685.
Solenthaler, C., 1990. On dislocation reactions in F.C.C. Σ3 twin boundaries. Materials Science and Engineering: A 125, 57–66.
Steinmetz, D.R., Jäpel, T., Wietbrock, B., Eisenlohr, P., Gutierrez-Urrutia, I., Saeed–Akbari, A., Hickel, T., Roters, F., Raabe, D., 2013. Revealing the strain-hardening behavior of twinning-induced plasticity steels: Theory, simulations, experiments. Acta Materialia 61, 494–510.
Stroh, A.N., 1958. Dislocations and Cracks in Anisotropic Elasticity. The Philosophical Magazine: A. Journal of Theoretical Experimental and Applied Physics 3, 625–646.
Stukowski, A., 2009. Visualization and analysis of atomistic simulation data with OVITO–the Open Visualization Tool. Modelling and Simulation in Materials Science and Engineering 18, 15012-15012.
Tadmor, E.B., Bernstein, N., 2004. A first-principles measure for the twinnability of FCC metals. Journal of the Mechanics and Physics of Solids 52, 2507–2519.
Ting, T.C.t., 1996. Anisotropic elasticity: theory and applications. Oxford University Press, New York.
Valentino, G.M., Xiang, S., Ma, L., Xie, K.Y., He, M.-R., Oliver, W.C., Pharr, G.M., Krogstad, J.A., Weihs, T.P., Hemker, K.J., 2021. Investigating the compressive strength and strain localization of nanotwinned nickel alloys. Acta Materialia 204, 116507.
Venables, J.A., 1961. Deformation twinning in face-centred cubic metals. The Philosophical Magazine: A. Journal of Theoretical Experimental and Applied Physics 6, 379–396.
Venables, J.A., 1964. The electron microscopy of deformation twinning. Journal of Physics and Chemistry of Solids 25, 685–692.
Vitek, V., 1992. Structure of dislocation cores in metallic materials and its impact on their plastic behaviour. Progress in Materials Science 36, 1–27.
Vítek, V., 1968. Intrinsic stacking faults in body-centred cubic crystals. The Philosophical Magazine: A. Journal of Theoretical Experimental and Applied Physics 18, 773–786.
Volterra, V., 1907. Sur l'équilibre des corps élastiques multiplement connexes. Annales scientifiques de l'École Normale Supérieure 24, 401–517.
Wang, J., Beyerlein, I.J., Tomé, C.N., 2014. Reactions of lattice dislocations with grain boundaries in Mg: Implications on the micro scale from atomic-scale calculations. International Journal of Plasticity 56, 156–172.
Wang, J., Misra, A., Hoagland, R.G., Hirth, J.P., 2012. Slip transmission across fcc/bcc interfaces with varying interface shear strengths. Acta Materialia 60, 1503–1513.
Wang, J., Sehitoglu, H., 2013. Twinning stress in shape memory alloys: Theory and experiments. Acta Materialia 61, 6790–6801.
Wang, P., Xu, S., Liu, J., Li, X., Wei, Y., Wang, H., Gao, H., Yang, W., 2017. Atomistic simulation for deforming complex alloys with application toward TWIP steel and associated physical insights. Journal of the Mechanics and Physics of Solids 98, 290–308.
Wei, D., Zaiser, M., Feng, Z., Kang, G., Fan, H., Zhang, X., 2019. Effects of twin boundary orientation on plasticity of bicrystalline copper micropillars: A discrete dislocation dynamics simulation study. Acta Materialia 176, 289–296.
Wu, Y., Bönisch, M., Alkan, S., Abuzaid, W., Sehitoglu, H., 2018. Experimental determination of latent hardening coefficients in FeMnNiCoCr. International Journal of Plasticity 105, 239–260.
Xu, S., Xiong, L., Chen, Y., McDowell, D.L., 2016. Sequential slip transfer of mixed-character dislocations across Σ3 coherent twin boundary in FCC metals: a concurrent atomistic-continuum study. npj Computational Materials 2, 15016.
Yamakov, V., Wolf, D., Phillpot, S.R., Gleiter, H., 2003. Dislocation–dislocation and dislocation–twin reactions in nanocrystalline Al by molecular dynamics simulation. Acta Materialia 51, 4135–4147.
Zhang, X., Lu, S., Zhang, B., Tian, X., Kan, Q., Kang, G., 2021. Dislocation–grain boundary interaction-based discrete dislocation dynamics modeling and its application to bicrystals with different misorientations. Acta Materialia 202, 88–98.
Zhao, G.-H., Xu, X., Dye, D., Rivera-Díaz-del-Castillo, P.E.J., 2020. Microstructural evolution and strain-hardening in TWIP Ti alloys. Acta Materialia 183, 155–164.
Zhu, T., Li, J., Samanta, A., Kim, H.G., Suresh, S., 2007. Interfacial plasticity governs strain rate sensitivity and ductility in nanostructured metals. Proceedings of the National Academy of Sciences 104, 3031.
Zhu, Y.T., Wu, X.L., Liao, X.Z., Narayan, J., Kecskés, L.J., Mathaudhu, S.N., 2011. Dislocation–twin interactions in nanocrystalline fcc metals. Acta Materialia 59, 812–821.
Zimmerman, J.A., Gao, H., Abraham, F.F., 2000. Generalized stacking fault energies for embedded atom FCC metals. Modelling and Simulation in. Materials Science and Engineering 8, 103–115.